This project has received funding from the Euratom research and training programme 2014-2018 under grant agreement No 662287.

EJP-CONCERT

European Joint Programme for the Integration of Radiation Protection Research

H2020 – 662287

D9.95 - Evaluating radiation effects on EV phenotype and cargo

PHE, NNK and HMGU

(Christophe Badie, Lourdes Cruz-Garcia, Eric Andreas Rutten, Katalin Lumniczky, Eszter Persa, Soile Tapio, Prabal Subedi)

Reviewer(s): Géza Sáfrány
and CONCERT coordination team

Work package / Task	**WP9**	**T9.5**	**ST9.5.2**
Deliverable nature:	**Report**		
Dissemination level: (Confidentiality)	**Public**		
Contractual delivery date:	**M48**		
Actual delivery date:	**M55 (with postponement)**		
Version:	**1**		
Total number of pages:	**30**		
Keywords:	**ionizing radiation (IR), Extracellular vesicles (EVs), phenotype and cargo**		
Approved by the coordinator:	**M55**		
Submitted to EC by the coordinator:	**M55**		

Abstract

The main objective of the deliverable was to determine how irradiation affects extracellular vesicles (EVs) phenotype and cargo. Bone marrow and plasma derived EVs were isolated from mice 24h after total-body irradiated (TBI) with a low dose (0.1 Gy) and with a high dose (3 Gy) and sent from NNK to PHE for miRNA analysis and to HMGU for proteomics. Phenotype analysis were performed in NNK.

The results demonstrated that ionizing radiation (IR) modifies the miRNA EVs content but presenting similar miRNA expression patterns at low and high doses only with the difference of the order of magnitude. The miRNAs cargo also showed a clear dose-dependency for the majority of the differentially expressed miRNAs.

Proteomic profiling of the EVs revealed radiation-induced changes in both the serum- and bone marrow-derived EVs. In the serum-derived EVs, 63 proteins were commonly deregulated at both radiation doses. In the bone marrow-derived EVs, 55 proteins were commonly deregulated. Most of the deregulated proteins were characterised as stress, defense or stimulus responsive. Both EV types shared 15 common differentially regulated proteins at both radiation doses but the direction of deregulation was not always similar. For example, fibrinogens were downregulated in the serum EVs but upregulated in the bone marrow EVs. However, similar pathways and upstream regulators were predicted when the deregulated proteins from both EV types were subjected to pathway analysis. The most important canonical pathway was acute phase response signalling.

EVS were analysed by flow cytometry in order to identify origin of EV-secreting cells. EVs were labelled against EV-specific and BM-specific proteins. Mesenchymal stem cells (MSCs) released the highest amount of EVs but EV production in these cells was not affected by irradiation. Hematopoietic stem cells (HSCs), erythroid and granulocyte progenitors released less EVs in control mice compared to MSCs, nevertheless, high dose irradiation resulted in increased EV-secretion of these cells.

To summarise, we showed that EVs miRNA and protein cargo is affected by IR. miRNAs profiles showed dose-dependency for groups of miRNAs in plasma and bone marrow. Proteomics analysis indicates a rapid change in the EV cargo reflecting possible alterations in the metabolic and inflammatory status of the donor cells. The main EVs producers are MSCs cells although IR affects the release only in HSCs, erythroid and granulocyte progenitors.

TABLE OF CONTENT

Introduction

Extracellular vesicles (EVs) are major mediators of bystander signals by carrying miRNAs and proteins and transferring their content into recipient cells and inducing changes in their cellular behavior. These EVs also carry cell surface proteins from their donor cells due to their biogenesis through budding of the plasma membrane or endosomal system. EVs phenotyping and cargo characterization will provide novel aspects of radiation-induced potential regulatory effects on recipient cells, bystander signalling mechanisms and information about the cells of origin.

The objective of the present deliverable is to study how irradiation affects EV phenotype and cargo. The deliverable will present data on the following investigations:

- Characterization of cargo of EVs from bone marrow and plasma of directly irradiated animals: miRNA and proteomic analysis
- Phenotypical characterization of bone marrow-derived EVs from directly irradiated animals

1. miRNA analysis of EVs cargo from bone marrow and plasma directly irradiated animals

Methods

10-12 week old male mice were irradiated with low dose (0.1 Gy) or high dose (3 Gy) X-rays. EVs were isolated from bone marrow and plasma 24 h after TBI with the ExoQuick-TC™ kit (System Biosciences). Total RNA was extracted using QIAGEN RNeasy mini kit and the miRNA content measured using the BioAnalyzer 2100 (Agilent technologies). For bone marrow-derived EVs, miRNA profiling was performed by using nCounter technology (NanoString Technologies) by running the samples in a mouse miRNA panel targeting 800 different miRNAs. We analyzed the results using a bioinformatics software, BRB-Array[1] tools in order to identify miRNAs responsive to ionizing radiation exposure. DIANA-miRPath v.3.0 software[2] was used to identify which pathways are targeted by the most represented miRNAs after irradiation. For the plasma-derived EVs, the miRNAs extracted were sequenced using an Illumina NextSeq 500 system by Arraystar (USA, http://www.arraystar.com/).

Results

a. miRNA profile of bone marrow-derived EVs from directly irradiated animals (0.1 Gy and 3 Gy)

The total RNA extracted from the bone marrow derived EVs from the 0 Gy, 0.1 Gy and 3 Gy groups was run in a nCounter panel which includes probes to identify 800 different murine miRNAs. The 0.1 Gy dose presented four significant upregulated miRNAs (Table 1) with fold changes ranging from 8 to 13-fold with p-values below 0.05. Pathway analysis of the top ten most significant up- and downregulated miRNAs from the 0.1 Gy dose (Table 2) showed that the most relevant miRNAs regulated by the low dose target genes are involved in endocytosis, cell cycle, MAPK signaling, Ubiquitin-mediated proteolysis, Leukocyte transendothelial migration, regulation of actin cytoskeleton and adherent junction.

Name	Group1	Group2	Fold Change	P-value	FDR
mmu-miR-761	2.00	13.00	4.67	0.03	1.00
mmu-miR-129-5p	3.00	18.00	4.75	0.04	1.00
mmu-miR-669g	2.00	10.00	3.67	0.05	1.00
mmu-miR-34b-5p	1.00	8.00	4.50	0.05	1.00

Table 1: Control vs 0.1 Gy significant miRNAs. Analysis performed with DIANA-miRPath v.3.0 software. Group1, control; Group2, 0.1 Gy; FDR, false discovery rate.

Upregulated miRNAs	Downregulated miRNAs
Endocytosis	Adherens junction
Cell cycle	Leukocyte transendothelial migration
MAPK signalling	Regulation of actin cytoskeleton
Ubiquitin-mediated proteolysis	

Table 2: Control vs 0.1Gy differentially regulated cellular pathways.

The 3 Gy dose showed a more extensive list of miRNAs regulated than at 0.1 Gy (Table 3). From the 20 miRNAs significantly regulated, only 2 were downregulated (mmu-miR-709 and mmu-miR 706). When comparing both doses, four different miRNAs were found to be statistically relevant in 0.1 Gy and 3 Gy: mmu-miR-761, mmu-miR-129-5p, mmu-miR-669g, and mmu-miR-34b-5p (Table 4). Therefore the 0.1 Gy response seems to be conserved in 3 Gy. All miRNAs have a higher fold change at 3Gy when compared to 0.1Gy, suggesting a dose-dependent upregulation, rather than an on/off mechanism of upregulation.

Pathway analyses of the 3 Gy group (Table 5) showed an extension of the pathways identified at 0.1 Gy. Some pathways are common target for the up and down regulated miRNAs suggesting different parts of the pathway being affected in different ways.

Name	Group1	Group2	Fold Change	P-value	FDR
mmu-miR-709	170.00	11.00	0.07	3.3e-4	0.08
mmu-miR-34b-5p	2.00	33.00	11.33	2.4e-3	0.20
mmu-miR-323-5p	2.00	40.00	13.67	2.6e-3	0.20
mmu-miR-761	3.00	34.00	8.75	4.9e-3	0.23
mmu-miR-291a-3p	3.00	32.00	8.25	5.3e-3	0.23
mmu-miR-323-3p	2.00	25.00	8.67	6.8e-3	0.23
mmu-miR-1946a	2.00	28.00	9.67	6.9e-3	0.23
mmu-miR-1933-5p	11.00	90.00	7.58	9.9e-3	0.29
mmu-miR-1898	3.00	30.00	7.75	0.01	0.29
mmu-miR-669g	3.00	26.00	6.75	0.01	0.29
mmu-miR-695	5.00	51.00	8.67	0.01	0.29
mmu-miR-706	32.00	4.00	0.15	0.02	0.30
mmu-miR-669h-5p	15.00	98.00	6.19	0.02	0.38
mmu-miR-338-5p	12.00	61.00	4.77	0.03	0.54
mmu-miR-466k	2.00	19.00	6.67	0.04	0.54
mmu-miR-1942	17.00	84.00	4.72	0.04	0.58
mmu-miR-129-5p	4.00	32.00	6.60	0.04	0.58
mmu-miR-688	6.00	33.00	4.86	0.05	0.60
mmu-miR-878-5p	8.00	44.00	5.00	0.05	0.60
mmu-miR-1904	6.00	42.00	6.14	0.05	0.60

Table 3. Control vs 3 Gy significantly differentially expressed miRNA. Analysis performed with DIANA-miRPath v.3.0 software. Group1, control; Group2, 3 Gy; FDR, false discovery rate.

miRNA	Fold change at 0.1Gy	Fold change at 3Gy
mmu-miR-761	4.67	8.75
mmu-miR-129-5p	4.75	6.60
mmu-miR-669g	3.67	6.75
mmu-miR-34b-5p	4.50	11.33

Table 4. Comparison of the miRNA profiles between 0.1 Gy and 3 Gy.

Upregulated miRNAs	Downregulated miRNAs	
Endocytosis	Adherens junction	Pathways in cancer
Cell cycle	Leukocyte transendothelial migration	mTOR signalling pathway
MAPK signalling	Regulation of actin cytoskeleton	Acute myeloid leukaemia
Ubiquitin-mediated proteolysis	Fatty acid biosynthesis	Wnt signalling pathway
Regulation of actin cytoskeleton	Proteoglycans in cancer	Transcriptional misregulation in cancer
Phosphatidylinositol signalling system	Lysine degradation	FoxO signalling pathway
D-glutamine and D-glutamate metabolism	N-Glycan biosynthesis	
Inositol phosphate metabolism	Protein processing in ER	
T cell receptor signalling pathway	Hippo signalling pathway	

Table 5. Control vs 3 Gy differentially regulated cellular pathways.

Clustering analysis performed with BRB array[1] tools showed clear up- and downregulated clusters of miRNAs which include the miRNAs identified using Diana tools software (Figure 1 and 2). These results demonstrate that the miRNA cargo of the EVs is modulated by irradiation and their response is not random. Besides, dose correlation analysis identified 13 miRNAs which show a strong dose-response (Table 6) with correlation coefficients between 0.95 and 0.84.

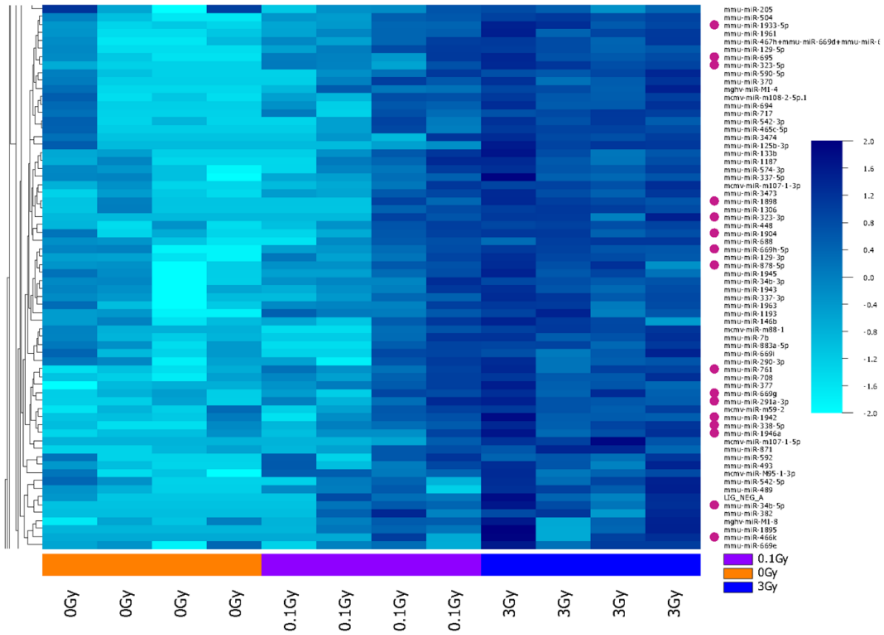

Figure 1. Heatmap and cluster dendrogram showing a cluster of upregulated miRNAs from bone marrow EVs from total body irradiated animals. Pink dots highlight the upregulated miRNAs identified by Diana tools in the previous tables.

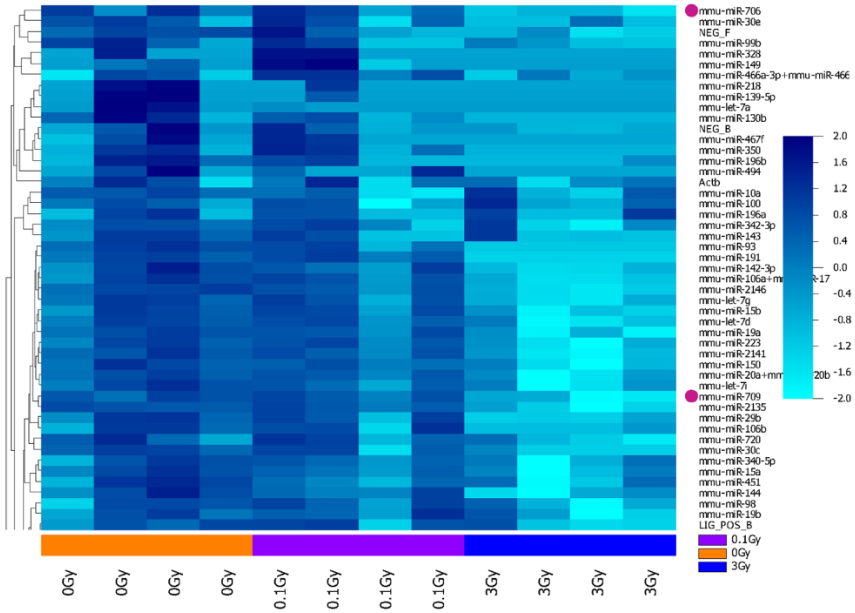

Figure 2. Heatmap and cluster dendrogram showing a cluster of downregulated miRNAs from bone marrow EVs from total body irradiated animals. Pink dots highlight the downregulated miRNAs identified by Diana tools in the previous tables.

Genes significantly correlated with Quantitative Trait:

Table - Sorted by p-value of the univariate test
The first 13 genes are significant at the nominal 0.001 level of the univariate test

	Correlation coefficient	Parametric p-value	FDR	UniqueID
1	0.953	< 1e-07	< 1e-07	mmu-miR-323-5p
2	0.888	9.17e-05	0.00592	mmu-miR-1933-5p
3	0.888	9.17e-05	0.00592	mmu-miR-1961
4	0.888	9.17e-05	0.00592	mmu-miR-338-5p
5	0.888	9.17e-05	0.00592	mmu-miR-504
6	0.884	0.0001922	0.0103	mcmv-miR-m107-1-5p
7	0.875	0.0003089	0.0125	mmu-miR-290-5p
8	0.874	0.0003089	0.0125	mmu-miR-708
9	0.857	0.0005971	0.0161	mmu-miR-181c
10	-0.857	0.0005971	0.0161	mmu-miR-2146
11	0.859	0.0005971	0.0161	mmu-miR-467h+mmu-miR-669d+mmu-miR-669l
12	0.857	0.0005971	0.0161	mmu-miR-669j
13	-0.843	0.0009695	0.0222	mmu-miR-93

Table 6. miRNAs correlated with the dose. BRB array tools correlation analyses showed 11 miRNAs positively and 2 negatively correlated with dose.

b. miRNA profile of plasma-derived EVs from directly irradiated animals

The miRNA profiling in plasma EVs was more challenging than in bone marrow EVs due to the miRNA concentrations obtained. Plasma and serum were pooled together from 12-25 animals and the EVs were extracted and then the total RNA. Plasma and serum were compared for miRNA content using a Bioanalyzer (Table 7) and the miRNA concentrations were too low to perform nCounter analyses for both types of samples. nCounter analyses require a concentration of 3.5 ng/ul and we obtained concentrations ranging from 0.07 to 0.6. Previous efforts to concentrate samples with a SpeedVac (DNA 120 SpeedVac, Thermo Savant) led to the loss of a significant part of the sample.

After total RNA extraction from plasma and serum, we observed that the serum miRNA content was even lower than plasma (Table 7), so we decided to continue only with plasma. Therefore, to be able to obtain miRNA information, we decided to perform sequencing instead of nCounter analyses. The sequencing analyses were outsourced to Arraystar (USA). Next-generation sequencing was performed in an Illumina NextSeq 500 system and miRDeep2 software was used to quantify known miRNA and differentially expressed miRNA were filtered using R package edgeR.

	Bioanalyzer Conc. [pg/µl]	30ul elution ng/ul	**Total left 28ul ng**
Plasma 0Gy	526.8	0.5268	**14.75**
Plasma 0.1GY	617.8	0.6178	**17.3**
Plasma 3Gy	644.2	0.6442	**18.04**
Serum 0Gy	73.5	0.0735	2.06
Serum 0.1 Gy	96.9	0.0969	2.71
Serum 3Gy	116.8	0.1168	3.27

Table 7. miRNA concentrations obtained from plasma and serum EVs.

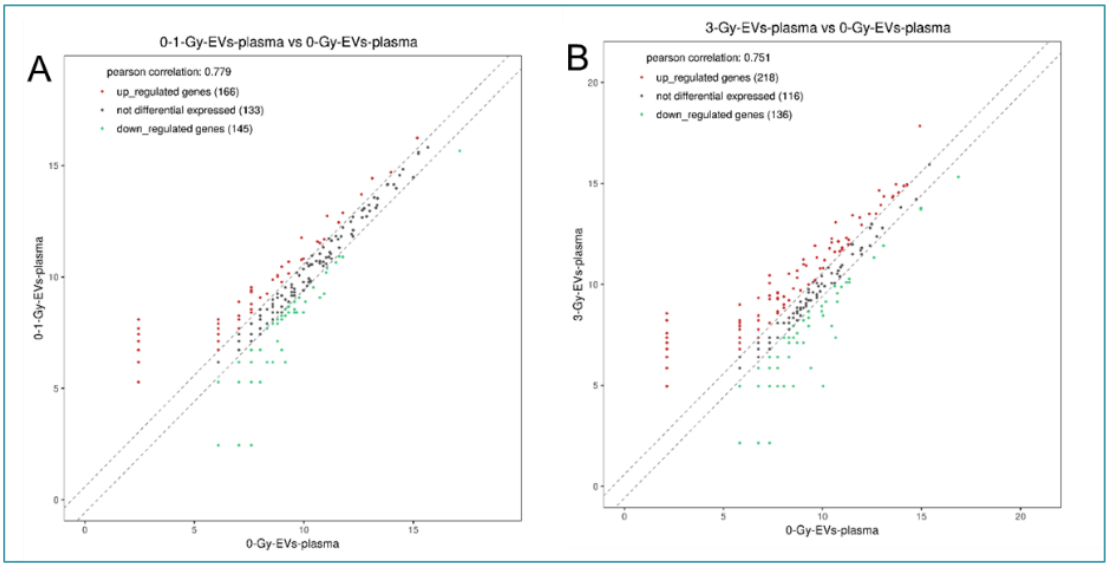

Figure 3. Differential expression scatterplots. The values of X and Y axes in the Scatter-Plot are the averaged CPM values of each group (log2 scaled). miRNAs above the top line (red dots, up-regulation) or below the bottom line (green dots, down-regulation) indicate more than 1.5-fold change between the two compared groups. Grey dots indicate non-differentially expressed miRNAs.

Differentially expressed analysis showed two miRNAs to be the highest upregulated miRNAs in both doses (Table 8), mmu-miR-378a-5p and 378b. It is known that miR-378a is embedded in the first intron of the ppargc1b gene encoding PGC-1β[3]. Both strands of miR-378a are coexpressed with PGC-1β; they may share the same transcriptional activators, and miR-378a might be involved in similar processes as PGC-1β. miR-378a targets genes involved in mitochondrial energy homeostasis, glycolysis, and skeletal muscle development and in tumor angiogenesis The sequence of miR-378a mature strands is highly conserved between species, with the miR-378a-5p strand being identical in both human and mice. miR-378b has a similar sequence as 378a but other localization.

Pathway analysis for miR-378b targets (Figure 4) identified acute myeloid leukemia pathway together with insulin and mTOR signaling pathways which are involved in cell metabolism, differentiation and survival. Pathway analysis including all the differentially upregulated miRNAs showed pathways (Fig. 5)

involved in several cancers together with metabolism, cell growth, proliferation, survival signaling pathways (PI3K/AKT pathway, mTOR, cAMP, Rap1, Ras) which are dysregulated in several types of cancer.

Top ten up regulated miRNAs
UP

0Gy versus 0.1Gy		0Gy versus 3Gy	
miRNA	Fold change	miRNA	Fold change
mmu-miR-378b	50.0	**mmu-miR-378b**	85.7
mmu-miR-378a-5p	37.8	**mmu-miR-378a-5p**	67.6
mmu-miR-335-3p	31.6	mmu-miR-696	43.4
mmu-miR-32-5p	25.5	mmu-miR-155-5p	37.3
mmu-miR-330-3p	25.5	mmu-miR-3068-3p	37.3
mmu-miR-7225-5p	25.5	mmu-miR-129-2-3p	31.3
mmu-miR-1195	19.4	mmu-miR-133a-5p	31.3
mmu-miR-135a-5p	19.4	mmu-miR-214-3p	31.3
mmu-miR-135a-5p	19.4	mmu-miR-34a-5p	31.3
mmu-miR-195a-3p	19.4	mmu-miR-125b-2-3p	25.2

Table 8. Top ten differentially expressed upregulated miRNAs in the 0.1 Gy and 3 Gy groups.

KEGG pathways

mmu-miR-378b

- Leukocyte transendothelial migration (mmu04670)
- Maturity onset diabetes of the young (mmu04950)
- Cocaine addiction (mmu05030)
- **Insulin signaling pathway** (mmu04910)
- **Acute myeloid leukemia** (mmu05221)
- **mTOR signaling pathway** (mmu04150)

mmu-miR-378a-5p

- Pyrimidine metabolism (mmu00240)
- Basal transcription factors (mmu03022)
- Bacterial invasion of epithelial cells (mmu05100)

Figure 4. Predicted KEGG pathways of the mmu-miR-37a and b gene targets. Analysis were performed with Diana tools software.

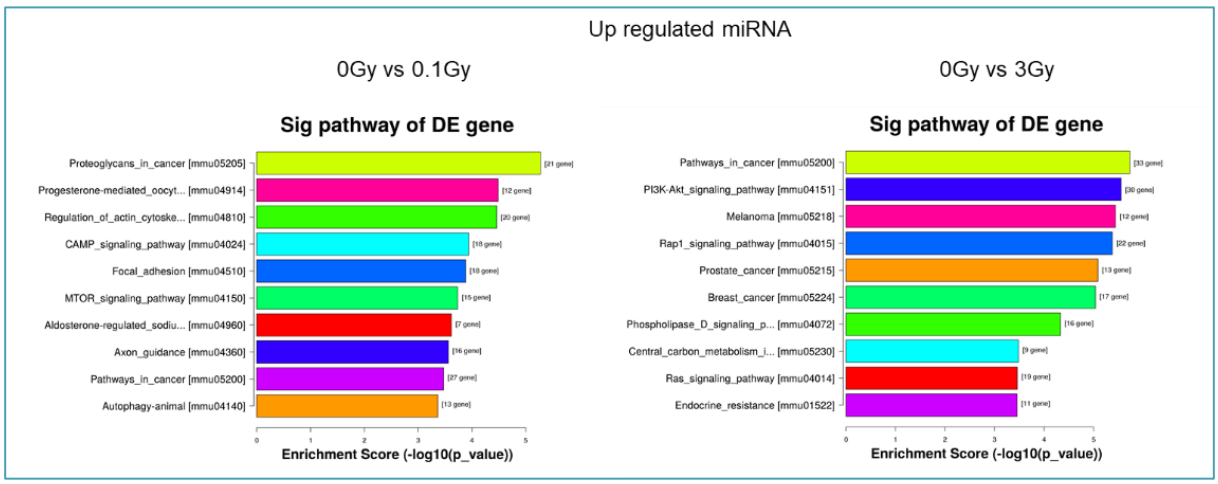

Figure 5. Top 10 significant pathways of the gene targets of the upregulated miRNAs. Ordered from top to bottom by P-value, with the most significant pathway on the top. The P-values calculated by Fisher's exact test are used to estimate the statistical significance of the enrichment of the pathways between the two groups.

The top ten differentially expressed downregulated miRNAs (Table 9) showed that common downregulated miRNAs are also present in both doses. Pathway analysis predicted pathways which might be potentiated due to the decrease of miRNAs targeting the genes involved in them (Figure 6). Within these pathways, there was MAPK, endocytosis, some cancers, cGMP-PKG and glycerophospholipids pathways amongst others.

Top ten down regulated miRNAs

Down

0Gy versus 0.1Gy		0Gy versus 3Gy	
miRNA	Fold change	miRNA	Fold change
mmu-miR-1968-5p	0.028	mmu-miR-6239	0.027
mmu-miR-223-5p	0.028	mmu-miR-6412	0.030
mmu-miR-106b-5p	0.042	mmu-miR-1895	0.041
mmu-miR-16-1-3p	0.042	mmu-miR-196a-5p	0.041
mmu-miR-1943-5p	0.042	mmu-miR-3102-3p	0.041
mmu-miR-196a-5p	0.042	mmu-miR-337-5p	0.041
mmu-miR-28a-5p	0.042	mmu-miR-365-1-5p	0.041
mmu-miR-28c	0.042	mmu-miR-676-5p	0.041
mmu-miR-3102-3p	0.042	mmu-miR-6934-3p	0.041
mmu-miR-365-1-5p	0.042	mmu-miR-6982-5p	0.041

Table 9. Top ten differentially expressed downregulated miRNAs in the 0.1 Gy and 3 Gy groups.

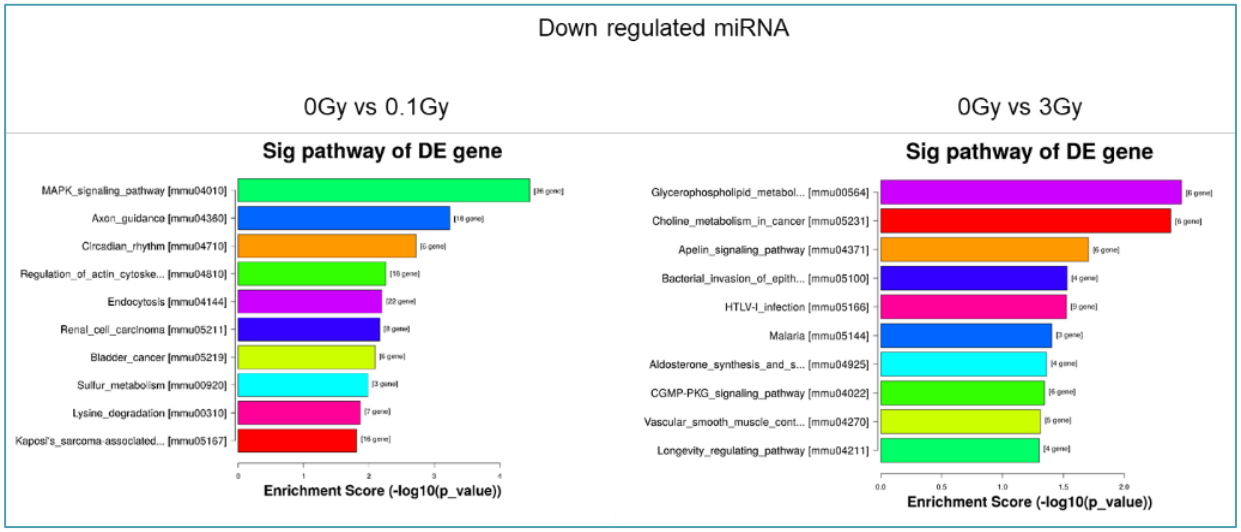

Figure 6. Top 10 significant pathways of the gene targets of the downregulated miRNAs. Ordered from top to bottom by P-value, with the most significant pathway on the top. The P-values calculated by Fisher's exact test are used to estimate the statistical significance of the enrichment of the pathways between the two groups.

Gene ontology analysis demonstrated that the genes that the miRNAs targeted in both doses are involved in similar biological processes with similar functions (Figure 7). Hierarchy clustering analysis were performed taking together all the miRNA identified by sequencing (Figure 8). The analysis presented dose-dependent upregulated and downregulated clusters of miRNAs. Selected miRNAs from these clusters were individually presented in Figure 9 demonstrating a strong dose-dependency.

0 Gy versus 0.1 Gy	0 Gy versus 3 Gy
Biological Process • Regulation of nitrogen compound metabolic process • Regulation of cellular metabolic process • Negative regulation of cellular process	**Biological Process** • Regulation of cellular metabolic process • Regulation of nitrogen compound metabolic process • Regulation of cellular process
Cellular Component • Cell • intracellular • Intracellular organelle	**Cellular Component** • Intracellular • Cell • Intracellular organelle
Molecular Function • Peptide binding • Amide binding • Protein binding	**Molecular Function** • Peptide binding • Amide binding • Protein binding

Figure 7. Gene ontology analysis of the upregulated miRNAs. Top 3 terms of each category for the 0.1 Gy and 3Gy groups.

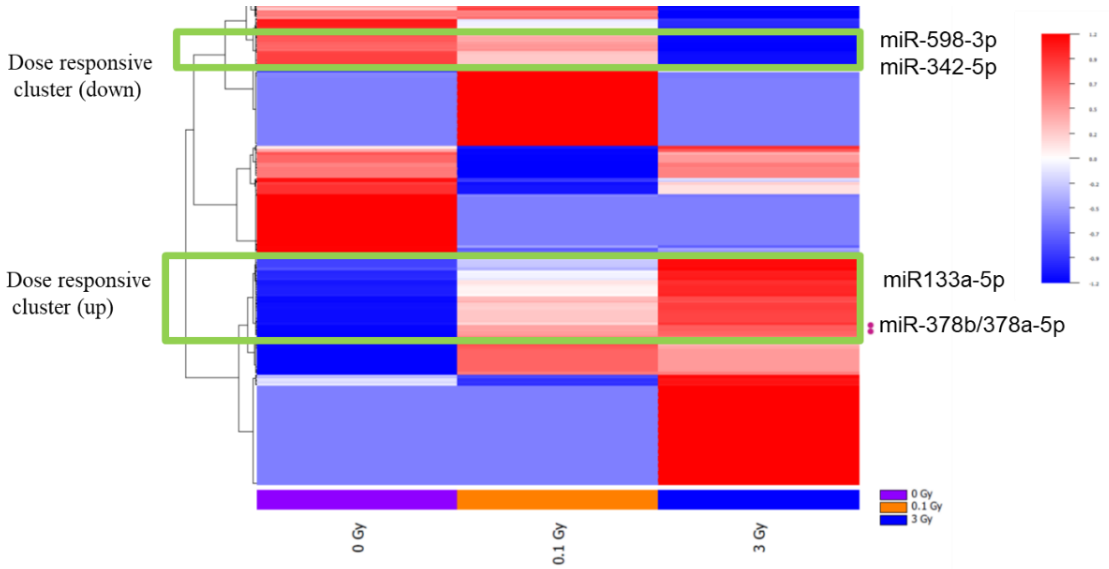

Figure 8. Heatmap and cluster dendrogram of the miRNAs sequencing data from plasma EVs from total body irradiated animals. Pink dots highlight the highest upregulated miRNAs identified mmu-miR-378n and 378a-5p.

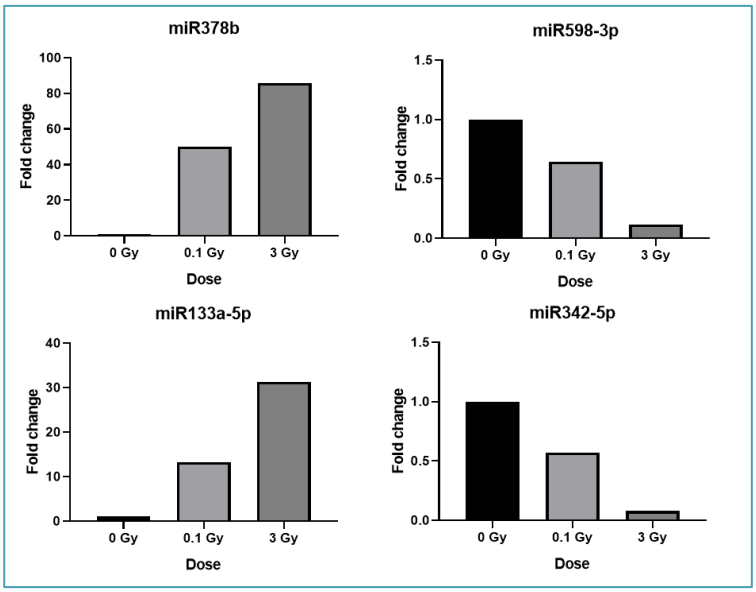

Figure 9. Selected dose-responsive miRNAs: miR-378b, miR-133a-5p, miR-598-3p and miR-342-5p.

Conclusion

Our data show that miRNA response does not operate in a binary fashion, either upregulated or downregulated by ionising radiation; it instead appears to be correlated to dose. As dose increases, more pathways are involved via IR-induced modifications to miRNA expression. The results suggest that IR induces similar miRNA expression patterns at low and high doses (only differences at the level of regulation-lower fold changes at lower dose) and their level of expression is dose-dependent for some of them. Therefore, the miRNAs dose response at 0.1 Gy is not qualitatively different to 3Gy, as much as it is more limited in bone marrow EVs as well as plasma EVs.

The dose response at 3 Gy expands upon an initial limited response at 0.1 Gy; it is likely the pathways upregulated at 0.1 Gy are triggered at a lower dose response than those only activated at 3 Gy. Clustering analysis identified clusters of miRNAs which showed a strong dose-dependency, therefore miRNA response is not random.

Pathway analysis showed cell differentiation, growth, proliferation and metabolism related pathways to be the common miRNAs targets for both doses. Dysregulation of these pathways are common in several cancers.

2. Proteomic analysis of EVs cargo from bone marrow and plasma directly irradiated animals

Introduction

Bystander signalling is a phenomenon where non-irradiated cells exhibit radiation-response-like effects resulting from signals received from (neighbouring) irradiated cells. Bystander signalling can be mediated through gap junctions[4], reactive oxygen species[5], or secretome[6]. Recently, EVs, sub-micron-sized cell-derived particles, are being studied for their role in mediating radiation-induced bystander signals[7 8]. To understand how EVs could mediate this, we have investigated the changes in the protein cargo of EVs derived from serum and bone marrow of total body irradiated mice.

Methods

Male, 10 – 12-week old CBA/H mice were total body irradiated (TBI) at NKK with 0 Gy (sham-irradiated control) 0.1 Gy, or 3 Gy using an X-ray source. EVs were collected from serum and bone marrow 24 h after TBI using ultracentrifugation.

At HMGU, the serum-derived EVs were lysed with radio immunoprecipitation buffer, trypsinised according to an in-house FASP protocol and the peptides were separated and identified using high-performance liquid chromatography coupled to a mass spectrometer (MS) (QExactive™ HF, ThermoFisher, Bremen, Germany). In the case of bone marrow-derived EVs, the trypsin digestion was performed in polyacrylamide gels (in-gel-digestion). The raw files from MS/MS were analysed using Proteome Discoverer 2.2 (ThermoFisher, Bremen, Germany) using 1 % false discovery rate (FDR). For identifying deregulated proteins, a fold change cut-off of $\pm$1.3 was applied to proteins that were identified with at least two unique peptides.

Results

In the serum-derived EVs, 310 proteins were identified in total. In the bone marrow-derived EVs, 2103 proteins were identified in total. In the serum- and bone marrow-derived EVs, 243 proteins and 1772 proteins were identified with at least two unique peptides, respectively.

No clustering was observed in principal component analysis (PCA) based on the protein abundances in serum-derived EVs (Figure 10). In contrast, the proteome features representing bone marrow-derived EVs from 0 Gy and 3 Gy treated mice showed clustering with the dose (Figure).

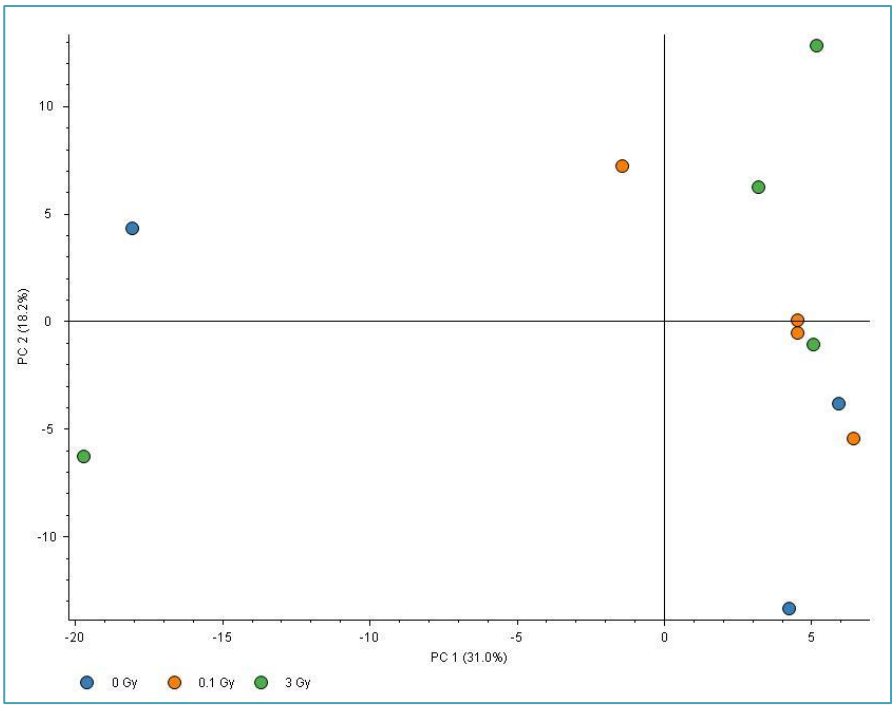

Figure 10. Principal component analysis (PCA) of serum derived-EVs from sham-irradiated mice (0 Gy) and irradiated mice (0.1 Gy and 3 Gy) based on protein abundances.

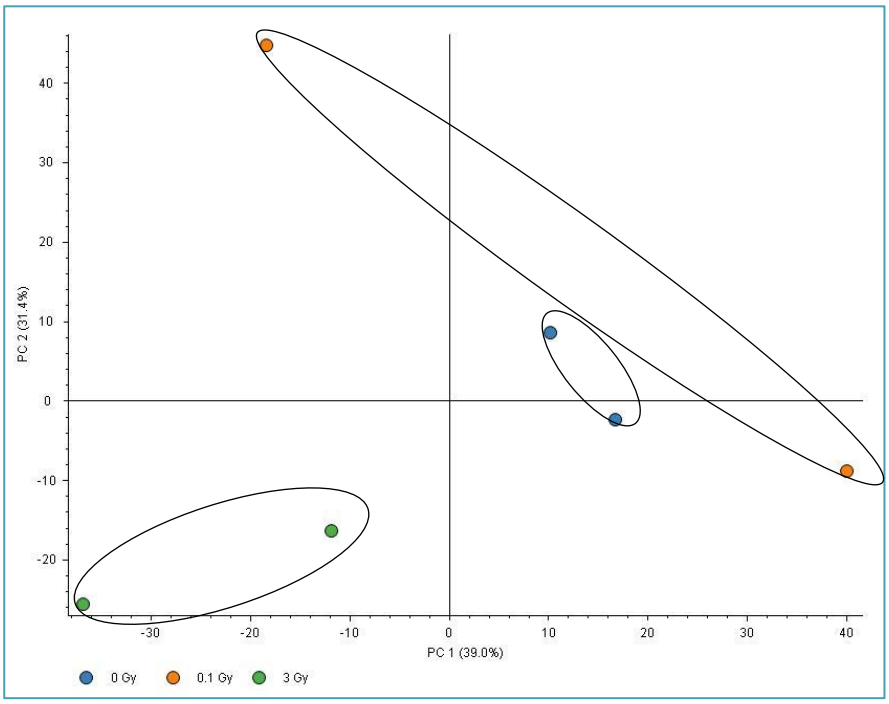

Figure 11. Principal component analysis (PCA) of bone marrow EVs from sham-irradiated mice (0 Gy) and irradiated mice (0.1 Gy and 3 Gy) based on protein abundances. Biological replicates for each dose are grouped and indicated by ellipses.

In the serum-derived EVs from mice treated with 0.1 Gy, 91 proteins were deregulated (57 downregulated, 34 upregulated) using a fold change cut-off of ±1.3. With a similar cut-off, 106 proteins were deregulated (62 downregulated and 44 upregulated) after 3 Gy treatment (Table 10.). There was no significant dose-dependent increase in the number of deregulated proteins.

Amongst the deregulated proteins, 63 proteins were common at both radiation doses. This represents 47% of all deregulated proteins. Only in two cases the direction of deregulation was opposite at these two doses.

The 63 common deregulated proteins were subjected to an *in silico* enrichment analysis (**Fehler! Verweisquelle konnte nicht gefunden werden.**) with the STRING web tool (https://string-db.org/). One major cluster and two minor clusters were observed, the major one representing mainly proteins belonging to defence or stress responses or responses to a stimulus.

Protein Accession	Description	Fold Change (0.1 Gy)	Fold Change (3 Gy)
Q80YY7	Zinc finger protein 618 OS=Mus musculus GN=Znf618 PE=2 SV=3	1.62	0.747
Q9D6F9	Tubulin beta-4A chain OS=Mus musculus GN=Tubb4a PE=1 SV=3	0.01	2.50
P35441	Thrombospondin-1 OS=Mus musculus GN=Thbs1 PE=1 SV=1	0.718	0.566
Q8QZY6	Tetraspanin-14 OS=Mus musculus GN=Tspan14 PE=1 SV=1	0.757	0.582
P26039	Talin-1 OS=Mus musculus GN=Tln1 PE=1 SV=2	0.512	0.512
P12246	Serum amyloid P-component OS=Mus musculus GN=Apcs PE=1 SV=2	1.52	1.32
P05367	Serum amyloid A-2 protein OS=Mus musculus GN=Saa2 PE=1 SV=1	9.95	10.4
P05366	Serum amyloid A-1 protein OS=Mus musculus GN=Saa1 PE=1 SV=2	9.28	14.7
Q91WP6	Serine protease inhibitor A3N OS=Mus musculus GN=Serpina3n PE=1 SV=1	1.33	1.38
Q8R429	Sarcoplasmic/endoplasmic reticulum calcium ATPase 1 OS=Mus musculus GN=Atp2a1 PE=1 SV=1	100	100
Q00724	Retinol-binding protein 4 OS=Mus musculus GN=Rbp4 PE=1 SV=2	0.723	0.677
Q64374	Regucalcin OS=Mus musculus GN=Rgn PE=1 SV=1	100	100
O55234	Proteasome subunit beta type-5 OS=Mus musculus GN=Psmb5 PE=1 SV=3	1.78	1.76
O35955	Proteasome subunit beta type-10 OS=Mus musculus GN=Psmb10 PE=1 SV=1	0.52	0.450
P49722	Proteasome subunit alpha type-2 OS=Mus musculus GN=Psma2 PE=1 SV=3	0.285	0.390
O08742	Platelet glycoprotein V OS=Mus musculus GN=Gp5 PE=1 SV=1	1.42	1.90
P39876	Metalloproteinase inhibitor 3 OS=Mus musculus GN=Timp3 PE=1 SV=1	0.502	0.622
P45700	Mannosyl-oligosaccharide 1,2-alpha-mannosidase IA OS=Mus musculus GN=Man1a1 PE=1 SV=1	0.630	0.581
P04939	Major urinary protein 3 OS=Mus musculus GN=Mup3 PE=1 SV=1	0.639	0.763
Q5FW60	Major urinary protein 20 OS=Mus musculus GN=Mup20 PE=1 SV=1	1.57	1.38
P11589	Major urinary protein 2 OS=Mus musculus GN=Mup2 PE=1 SV=1	1.58	1.30
B5X0G2	Major urinary protein 17 OS=Mus musculus GN=Mup17 PE=2 SV=2	2.20	1.50
P11588	Major urinary protein 1 OS=Mus musculus GN=Mup1 PE=1 SV=1	1.55	1.48
P17897	Lysozyme C-1 OS=Mus musculus GN=Lyz1 PE=1 SV=1	0.329	0.524
Q61805	Lipopolysaccharide-binding protein OS=Mus musculus GN=Lbp PE=1 SV=2	0.424	0.351
Q8BGZ7	Keratin, type II cytoskeletal 75 OS=Mus musculus GN=Krt75 PE=1 SV=1	0.453	0.759
Q6NXH9	Keratin, type II cytoskeletal 73 OS=Mus musculus GN=Krt73 PE=1 SV=1	0.310	1.51

Q9R0H5	Keratin, type II cytoskeletal 71 OS=Mus musculus GN=Krt71 PE=1 SV=1	2.88	3.02
P07744	Keratin, type II cytoskeletal 4 OS=Mus musculus GN=Krt4 PE=1 SV=2	0.613	0.655
Q6IFZ6	Keratin, type II cytoskeletal 1b OS=Mus musculus GN=Krt77 PE=1 SV=1	1.42	1.63
Q02257	Junction plakoglobin OS=Mus musculus GN=Jup PE=1 SV=3	0.443	0.723
P01725	Ig lambda-1 chain V region S178 OS=Mus musculus PE=1 SV=1	0.510	0.587
P01843	Ig lambda-1 chain C region OS=Mus musculus PE=1 SV=1	0.573	0.667
P01637	Ig kappa chain V-V region T1 OS=Mus musculus PE=4 SV=1	0.681	0.595
P01655	Ig kappa chain V-III region PC 7132 OS=Mus musculus PE=1 SV=1	0.638	0.770
P01664	Ig kappa chain V-III region CBPC 101 OS=Mus musculus PE=1 SV=1	0.427	0.506
P01630	Ig kappa chain V-II region 7S34.1 OS=Mus musculus PE=1 SV=1	0.752	0.653
P01629	Ig kappa chain V-II region 2S1.3 OS=Mus musculus PE=1 SV=1	0.553	0.01
P01633	Ig kappa chain V19-17 OS=Mus musculus GN=Igk-V19-17 PE=1 SV=1	0.715	0.591
P01787	Ig heavy chain V regions TEPC 15/S107/HPCM1/HPCM2/HPCM3 OS=Mus musculus PE=1 SV=1	0.683	0.645
P06327	Ig heavy chain V region VH558 A1/A4 OS=Mus musculus GN=Gm5629 PE=2 SV=1	0.603	0.650
P01819	Ig heavy chain V region MOPC 141 OS=Mus musculus PE=4 SV=1	0.693	0.748
P01756	Ig heavy chain V region MOPC 104E OS=Mus musculus PE=1 SV=1	0.739	0.551
P18527	Ig heavy chain V region 914 OS=Mus musculus PE=1 SV=1	2.19	8.09
P18528	Ig heavy chain V region 6.96 OS=Mus musculus PE=4 SV=1	1.85	1.70
Q61646	Haptoglobin OS=Mus musculus GN=Hp PE=1 SV=1	2.00	1.31
P14426	H-2 class I histocompatibility antigen, D-K alpha chain OS=Mus musculus GN=H2-D1 PE=1 SV=1	0.638	0.522
P46412	Glutathione peroxidase 3 OS=Mus musculus GN=Gpx3 PE=1 SV=2	0.691	0.746
P13020	Gelsolin OS=Mus musculus GN=Gsn PE=1 SV=3	0.754	0.634
P05064	Fructose-bisphosphate aldolase A OS=Mus musculus GN=Aldoa PE=1 SV=2	1.64	1.47
Q8VCM7	Fibrinogen gamma chain OS=Mus musculus GN=Fgg PE=1 SV=1	0.648	0.419
Q8K0E8	Fibrinogen beta chain OS=Mus musculus GN=Fgb PE=1 SV=1	0.668	0.439
E9PV24	Fibrinogen alpha chain OS=Mus musculus GN=Fga PE=1 SV=1	0.611	0.513
P07310	Creatine kinase M-type OS=Mus musculus GN=Ckm PE=1 SV=1	100	100
P03953	Complement factor D OS=Mus musculus GN=Cfd PE=1 SV=1	1.31	1.44
Q8VCG4	Complement component C8 gamma chain OS=Mus musculus GN=C8g PE=1 SV=1	1.53	1.38
Q02105	Complement C1q subcomponent subunit C OS=Mus musculus GN=C1qc PE=1 SV=2	0.752	0.727
P40240	CD9 antigen OS=Mus musculus GN=Cd9 PE=1 SV=2	0.597	0.729
Q9WVJ3	Carboxypeptidase Q OS=Mus musculus GN=Cpq PE=1 SV=1	0.681	0.718
Q8CIF4	Biotinidase OS=Mus musculus GN=Btd PE=1 SV=2	0.616	0.686
Q9Z2W0	Aspartyl aminopeptidase OS=Mus musculus GN=Dnpep PE=1 SV=2	0.01	0.01
P11859	Angiotensinogen OS=Mus musculus GN=Agt PE=1 SV=1	1.407	1.35
P68033	Actin, alpha cardiac muscle 1 OS=Mus musculus GN=Actc1 PE=1 SV=1	1.45	1.83

Table 10. List of deregulated proteins (fold change > ±1.3) in serum-derived EVs

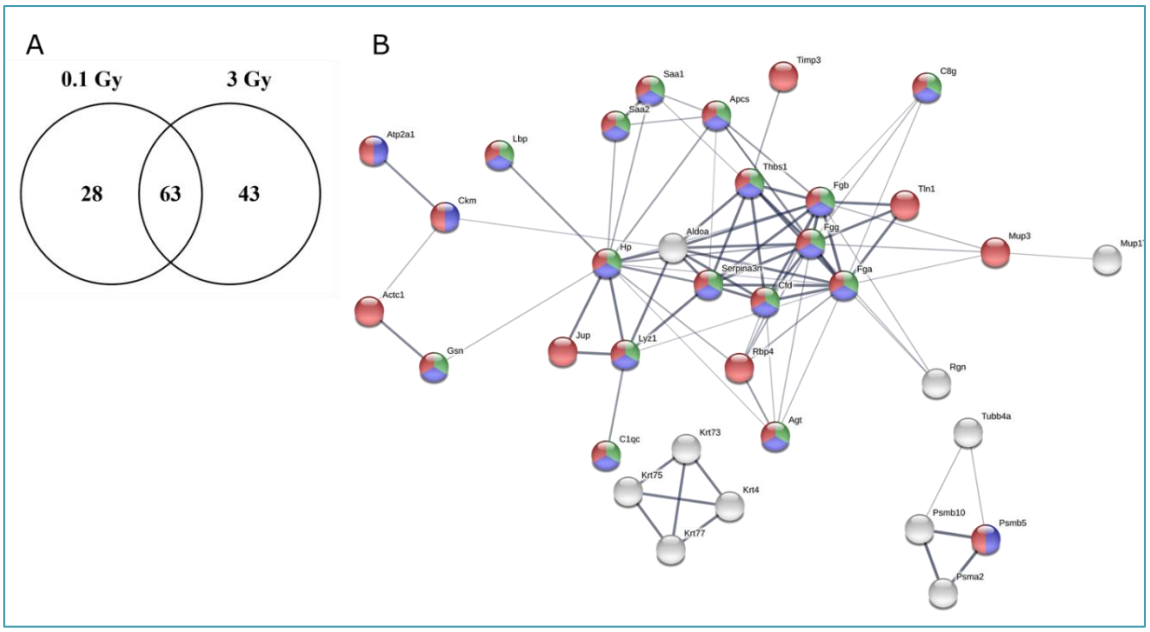

Figure 12. (A) A Venn diagram showing the number of deregulated proteins in serum-derived EVs from mice treated with 0.1 Gy or 3 Gy TBI. (B) STRING enrichment analysis of the 63 common deregulated proteins is shown. Proteins, belonging to defence response (GO:0006952, FDR 1.12×10^{-16}, green), response to stress (GO:0006950, FDR 1.12×10^{-6}, blue), and response to stimulus (GO:0050896, FDR 8.79×10^{-6}, red), are marked.

In the bone marrow derived EVs from the mice treated with 0.1 Gy, altogether 148 proteins were deregulated of which 5 were downregulated and 143 upregulated (Table 11). After the 3 Gy treatment, 152 proteins were deregulated (68 downregulated and 84 upregulated). Similar to serum-derived EVs, the number of deregulated proteins did not show dose-dependent increase. In total, 55 deregulated proteins were common in both treatment doses (**Fehler! Verweisquelle konnte nicht gefunden werden.**). This represents 23% of all deregulated proteins. In five cases, the direction of the deregulation was opposite at these two radiation doses.

The 55 common deregulated proteins were subjected to an *in silico* enrichment analysis (Figure 13) with the STRING web tool (https://string-db.org/). Similar to the serum-derived EVs, the STRING enrichment analysis revealed that these proteins formed two clusters, both representing mainly defence or stress responses or responses to a stimulus.

Protein Accession	Protein Description	Fold Change (0.1 Gy)	Fold Change (3 Gy)
P07724	Serum albumin OS=Mus musculus GN=Alb PE=1 SV=3	4.80	11.9
Q8K0E8	Fibrinogen beta chain OS=Mus musculus GN=Fgb PE=1 SV=1	8.18	25.2
Q8VCM7	Fibrinogen gamma chain OS=Mus musculus GN=Fgg PE=1 SV=1	3.60	12.4
P01872	Ig mu chain C region OS=Mus musculus GN=Ighm PE=1 SV=2	5.51	12.4
Q91X72	Hemopexin OS=Mus musculus GN=Hpx PE=1 SV=2	5.67	19.2
O08677	Kininogen-1 OS=Mus musculus GN=Kng1 PE=1 SV=1	5.92	27.8
P01878	Ig alpha chain C region OS=Mus musculus PE=1 SV=1	5.88	13.9
Q91WP6	Serine protease inhibitor A3N OS=Mus musculus GN=Serpina3n PE=1 SV=1	35.8	27.5
P26040	Ezrin OS=Mus musculus GN=Ezr PE=1 SV=3	9.98	11.3
Q8K182	Complement component C8 alpha chain OS=Mus musculus GN=C8a PE=1 SV=1	11.8	98.0
Q99KK7	Dipeptidyl peptidase 3 OS=Mus musculus GN=Dpp3 PE=1 SV=2	9.58	11.1
P09242	Alkaline phosphatase, tissue-nonspecific isozyme OS=Mus musculus GN=Alpl PE=1 SV=2	7.39	14.4
Q9QXC1	Fetuin-B OS=Mus musculus GN=Fetub PE=1 SV=1	100	100
Q08857	Platelet glycoprotein 4 OS=Mus musculus GN=Cd36 PE=1 SV=2	42.0	39.6
Q01279	Epidermal growth factor receptor OS=Mus musculus GN=Egfr PE=1 SV=1	100	100

Q9ESB3	Histidine-rich glycoprotein OS=Mus musculus GN=Hrg PE=1 SV=2	6.61	7.4
Q9JLV6	Bifunctional polynucleotide phosphatase/kinase OS=Mus musculus GN=Pnkp PE=1 SV=2	100	100
P08003	Protein disulfide-isomerase A4 OS=Mus musculus GN=Pdia4 PE=1 SV=3	17.9	48.6
Q80TP3	E3 ubiquitin-protein ligase UBR5 OS=Mus musculus GN=Ubr5 PE=1 SV=2	100	100
Q64337	Sequestosome-1 OS=Mus musculus GN=Sqstm1 PE=1 SV=1	100	100
Q8CD15	Bifunctional lysine-specific demethylase and histidyl-hydroxylase MINA OS=Mus musculus GN=Mina PE=1 SV=2	6.82	0.01
P11680	Properdin OS=Mus musculus GN=Cfp PE=2 SV=2	100	100
O70362	Phosphatidylinositol-glycan-specific phospholipase D OS=Mus musculus GN=Gpld1 PE=1 SV=1	100	100
P52432	DNA-directed RNA polymerases I and III subunit RPAC1 OS=Mus musculus GN=Polr1c PE=1 SV=3	100	100
Q8R121	Protein Z-dependent protease inhibitor OS=Mus musculus GN=Serpina10 PE=1 SV=1	100	100
Q8BH35	Complement component C8 beta chain OS=Mus musculus GN=C8b PE=1 SV=1	100	100
Q8BJ48	N-acetylglucosamine-1-phosphodiester alpha-N-acetylglucosaminidase OS=Mus musculus GN=Nagpa PE=1 SV=2	100	100
P05366	Serum amyloid A-1 protein OS=Mus musculus GN=Saa1 PE=1 SV=2	100	100
Q6NV83	U2 snRNP-associated SURP motif-containing protein OS=Mus musculus GN=U2surp PE=1 SV=3	100	100
P01801	Ig heavy chain V-III region J606 OS=Mus musculus PE=1 SV=1	16.9	38.9
Q99JR8	SWI/SNF-related matrix-associated actin-dependent regulator of chromatin subfamily D member 2 OS=Mus musculus GN=Smarcd2 PE=1 SV=2	9.59	0.01
P46467	Vacuolar protein sorting-associated protein 4B OS=Mus musculus GN=Vps4b PE=1 SV=2	100	100
O35343	Importin subunit alpha-3 OS=Mus musculus GN=Kpna4 PE=1 SV=1	100	100
Q9ESM6	Glycerophosphoinositol inositolphosphodiesterase GDPD2 OS=Mus musculus GN=Gdpd2 PE=1 SV=1	100	100
O35972	39S ribosomal protein L23, mitochondrial OS=Mus musculus GN=Mrpl23 PE=1 SV=1	12.3	0.01
P97300	Neuroplastin OS=Mus musculus GN=Nptn PE=1 SV=3	18.5	29.1
Q6P1B1	Xaa-Pro aminopeptidase 1 OS=Mus musculus GN=Xpnpep1 PE=1 SV=1	100	100
Q99JR1	Sideroflexin-1 OS=Mus musculus GN=Sfxn1 PE=1 SV=3	100	100
Q9JJK2	LanC-like protein 2 OS=Mus musculus GN=Lancl2 PE=1 SV=1	100	100
Q9DBR0	A-kinase anchor protein 8 OS=Mus musculus GN=Akap8 PE=1 SV=1	14.6	0.01
Q8K354	Carbonyl reductase [NADPH] 3 OS=Mus musculus GN=Cbr3 PE=1 SV=1	100	100
Q8K310	Matrin-3 OS=Mus musculus GN=Matr3 PE=1 SV=1	11.2	0.01
Q8C0L6	Peroxisomal N(1)-acetyl-spermine/spermidine oxidase OS=Mus musculus GN=Paox PE=1 SV=3	100	100
Q9QZF2	Glypican-1 OS=Mus musculus GN=Gpc1 PE=1 SV=1	100	100
Q8R2S8	CD177 antigen OS=Mus musculus GN=Cd177 PE=2 SV=1	100	100
Q80ZV0	Ribonuclease H2 subunit B OS=Mus musculus GN=Rnaseh2b PE=1 SV=2	100	100
Q00519	Xanthine dehydrogenase/oxidase OS=Mus musculus GN=Xdh PE=1 SV=5	100	100
Q8CIN4	Serine/threonine-protein kinase PAK 2 OS=Mus musculus GN=Pak2 PE=1 SV=1	100	100
Q8BTJ4	Bis(5'-adenosyl)-triphosphatase enpp4 OS=Mus musculus GN=Enpp4 PE=1 SV=1	15.5	27.8
P18654	Ribosomal protein S6 kinase alpha-3 OS=Mus musculus GN=Rps6ka3 PE=1 SV=2	11.5	0.01
P62915	Transcription initiation factor IIB OS=Mus musculus GN=Gtf2b PE=1 SV=1	100	100
P25976	Nucleolar transcription factor 1 OS=Mus musculus GN=Ubtf PE=1 SV=1	6.03	0.01
Q9Z183	Protein-arginine deiminase type-4 OS=Mus musculus GN=Padi4 PE=2 SV=3	100	100
P41241	Tyrosine-protein kinase CSK OS=Mus musculus GN=Csk PE=1 SV=2	100	100
Q8R3H7	Heparan sulfate 2-O-sulfotransferase 1 OS=Mus musculus GN=Hs2st1 PE=1 SV=2	100	100

Table 11. List of deregulated proteins (fold change > ±1.3) in bone marrow-derived EVs

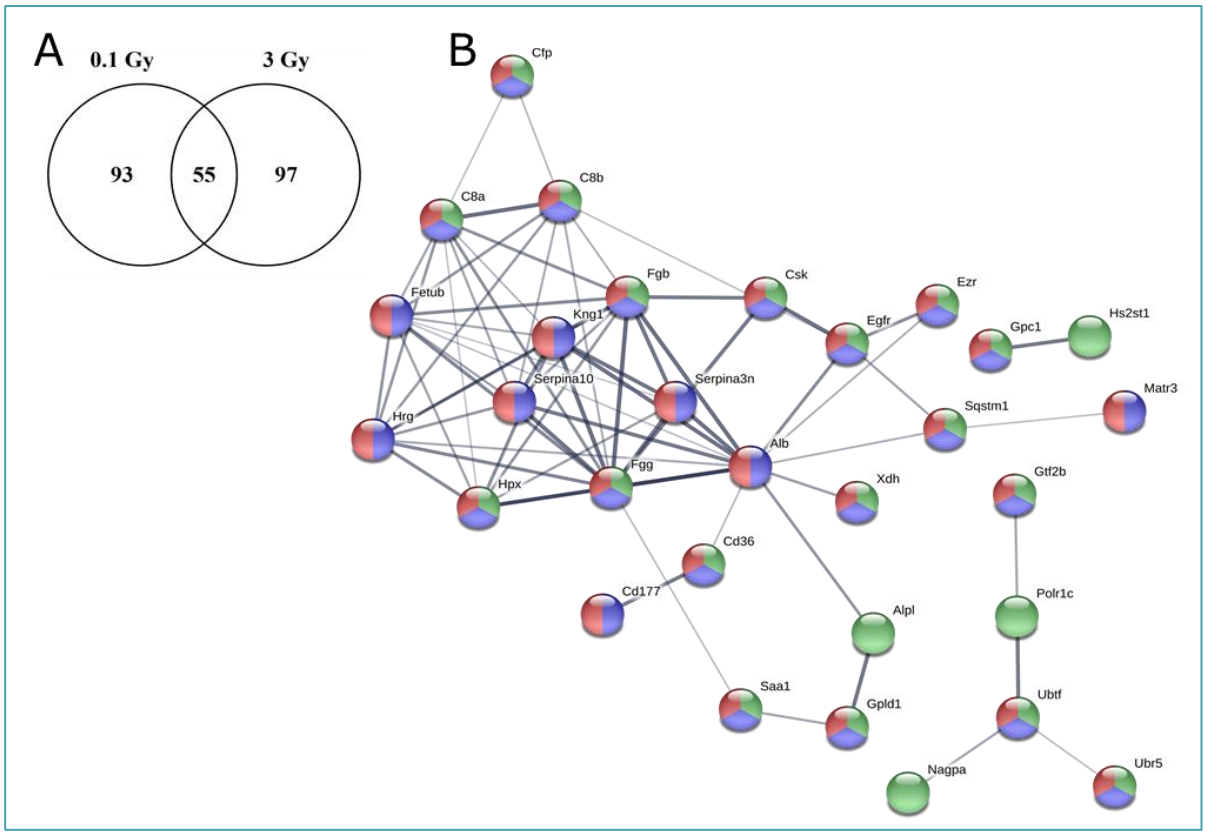

Figure 13. (A) A Venn diagram showing the number of deregulated proteins in bone marrow-derived EVs from mice treated with 0.1 Gy or 3 Gy TBI is shown. (B) STRING enrichment analysis of the 55 commonly deregulated proteins is illustrated. The proteins, belonging to defence response (GO:0006952, FDR 2.39×10^{-6}, green), response to stress (GO:0006950, FDR 2.39×10^{-6}, blue), and response to stimulus (GO:0050896, FDR 4.77×10^{-5}, red), were all upregulated with the exception of UBTF.

In both EV types and at both radiation doses there were 15 common differentially regulated proteins (Table 12). These did not always show similar direction of deregulation. For example, the fibrinogens were downregulated in the serum-derived EVs but upregulated in the bone marrow-derived EVs. These proteins represented similar groups as seen with the previous analyses of serum or bone marrow-derived EVs, namely proteins responding to stress or stimulus or participating in the cellular defence.

The shared deregulated proteins showed high level of clustering in the protein-protein interaction analysis (Figure 14). All proteins with the exception of angiotensin-converting enzyme (ACE) belonged to this cluster.

Accession	Protein Description	Fold change in serum-derived EVs		Fold change in bone marrow-derived EVs	
		0.1 Gy	3 Gy	0.1 Gy	3 Gy
P05366	Serum amyloid A-1 protein OS=Mus musculus GN=Saa1 PE=1 SV=2	7.67	20.1	100	100
Q91WP6	Serine protease inhibitor A3N OS=Mus musculus GN=Serpina3n PE=1 SV=1	-	1.55	35.8	27.5
Q9QUM0	Integrin alpha-IIb OS=Mus musculus GN=Itga2b PE=1 SV=2	-	0.699	7.13	-
P01801	Ig heavy chain V-III region J606 OS=Mus musculus PE=1 SV=1	0.604	0.707	16.88	38.9
Q8VCM7	Fibrinogen gamma chain OS=Mus musculus GN=Fgg PE=1 SV=1	0.562	0.406	3.60	12.4
Q8K0E8	Fibrinogen beta chain OS=Mus musculus GN=Fgb PE=1 SV=1	0.514	0.411	8.18	25.2
Q06770	Complement C4-B OS=Mus musculus GN=C4b PE=1 SV=3	-	0.614	-	15.6
P01029	Complement C4-B OS=Mus musculus GN=C4b PE=1 SV=3	0.74	-	-	6.48
Q00898	Alpha-1-antitrypsin 1-5 OS=Mus musculus GN=Serpina1e PE=1 SV=1	-	1.406	-	15.5
O89020	Afamin OS=Mus musculus GN=Afm PE=1 SV=2	-	0.739	-	54.8
P01878	Ig alpha chain C region OS=Mus musculus PE=1 SV=1	1.489	0.737	5.88	13.9
Q9QXC1	Fetuin-B OS=Mus musculus GN=Fetub PE=1 SV=1	-	-	100	100
Q8BH35	Complement component C8 beta chain OS=Mus musculus GN=C8b PE=1 SV=1	-	1.33	100	100
P09470	Angiotensin-converting enzyme OS=Mus musculus GN=Ace PE=1 SV=3	1.51	1.36	0.057	-
P29699	Alpha-2-HS-glycoprotein OS=Mus musculus GN=Ahsg PE=1 SV=1	-	0.688	-	9.53

Table 12. Common deregulated proteins in serum- and bone marrow-EVs

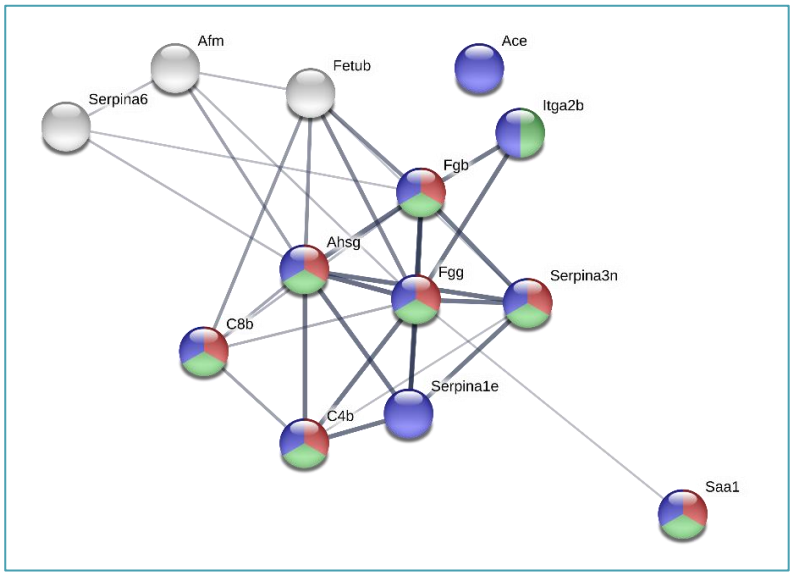

Figure 14. STRING enrichment analysis of the common deregulated proteins in serum- and bone marrow-derived EVs. Proteins belonging to defence response (GO:0006952, FDR 5.39 × 10^{-5}, red), response to stress (GO:0006950, FDR 0.0010, green), and response to stimulus (GO:0050896, FDR 0.0050, blue), are indicated.

All deregulated proteins in both bone marrow-derived and serum-derived EVs were imported in the Ingenuity Pathway Analysis (IPA). The deregulated proteins from both EV types represented similar predicted upstream regulators and canonical pathways (Figure). The most important predicted upstream regulators were IL6, TGF beta 1, HNF4A (hepatocyte nuclear factor 4 alpha), and dimeric STAT3. The most important canonical pathways were acute phase response signalling, LXR/RXR signalling, FXR/RXR signalling, and coagulation system. This analysis indicates a possible role of both EV types in rapid reprogramming of protein expression and metabolism in response to radiation-induced inflammatory cytokine signalling.

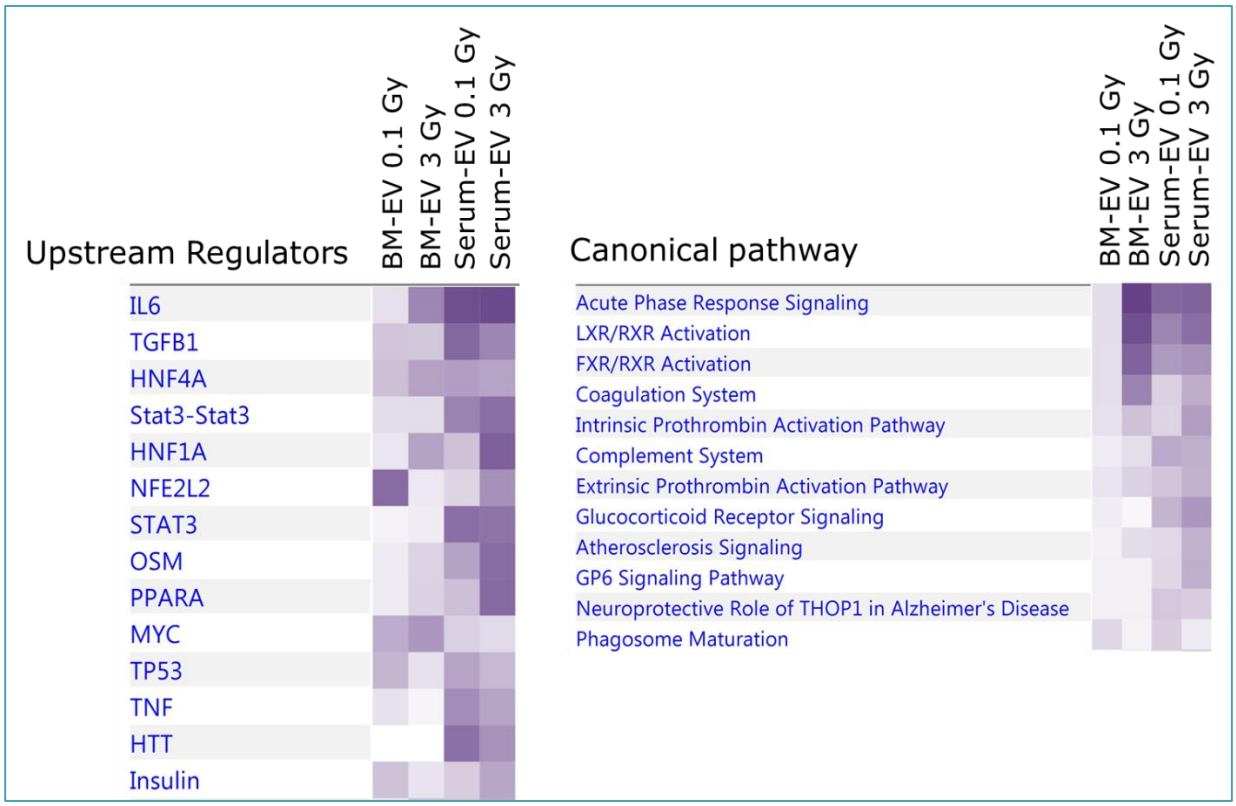

Figure 15. The predicted upstream regulators and canonical pathways for the deregulated proteins identified in both bone marrow-derived and serum-derived EVs (the darker the colour, the more accurate is the prediction). All coloured boxes have a p-value of ≤ 0.05; white boxes have a p-value of ≥ 0.05 meaning no significant alteration compared to the sham-irradiation.

Conclusions

The aim of this work was proteomic profiling of EVs from bone marrow and serum of directly irradiated animals in order to evaluate radiation effects on EV phenotype and cargo. A change in the proteome of the serum- and bone marrow-derived EVs was observed rapidly (24 h) after the mice were treated with 0.1 or 3 Gy TBI. No dose-dependent increase in the number of deregulated proteins was observed in either serum- or bone marrow-derived EVs. However, the number of common deregulated proteins between the two radiation doses was high, being 47% and 23% in serum- and bone marrow-derived EVs, respectively. *In-silico* protein−protein interaction analysis of the significantly differentially expressed proteins in either the serum- or bone marrow-derived EVs showed interconnected protein clusters representing mainly stress and acute phase response proteins. Moreover, similar pathways and upstream regulators were predicted for the serum and bone marrow-derived proteins.

3. Phenotypical characterization of bone marrow-derived EVs from directly irradiated

Introduction

EVs are small (50-1000 nm) membrane coated bodies, consisting of exosomes and microvesicles, actively released by most of the cell types[9]. Their cargo consists of RNA, microRNA (miRNA), protein and lipid molecules originating from the parental cell [10 11] and by traveling in the extracellular space and blood they transfer these signals and information to other distant cells [12 13] facilitating intercellular communication. EVs use different mechanisms for information transfer, including induction of receptor-mediated intracellular signal transduction by surface-expressed ligands, or delivering functional proteins, RNAs, and lipids into the target cells by fusion with plasma membrane or internalization into the endocytic compartment [14]. EVs are secreted by cells under physiological conditions and various disease states, as well. It is well-know that in cancerous microenvironment [15] or in systemic stress conditions, including ionizing irradiation[16], the release of extracellular vesicles is significantly increased. Irradiation can alter the composition of proteins and RNAs expressed by cells [17] and most probably also the type and amount of these macromolecules packed in the extracellular vesicles[18 8 19].

In this task of the actual deliverable we analysed the cell populations in BM which release EVs into the BM niche under healthy and irradiated conditions. Mice were irradiated and BM cell supernatant was collected followed by EV isolation using precipitation method. EVs were fluorescently labelled and surface proteins were measured by flow cytometry to obtain an immune phenotyping profile of EVs released by the different cellular components of the BM.

Methods

Handling conditions and irradiation procedure of animals

10-12 weeks old CBA male mice were used for EV isolation. Mice were kept and investigated in accordance with the guidelines and all applicable sections of the Hungarian and European 2010/63/EU directives and regulations. All animal studies were approved and permission was issued by Budapest and Pest County Administration Office Food Chain Safety and Animal Health Board. The number of the ethical permission: PE/EA/392-7/2017.

Five mice were irradiated simultanously by inserting them into a pie cage and subjected them to whole body irradiation with 0.1 and 3 Gy using a X-RAD 225/XLiX-ray source (Precision X-Ray, North Branford, United States). Irradiated and control animals were kept for 24 hours in their standard conditions, with food and water *ad libitum*. 24 hours later mice were sacrificed by i.p. injection 20 µL Euthanimal 40% solution (Alfasan, JaWoerden, The Netherlands).

Extraction of bone marrow cells (BMCs) and supernatant

After dissection the legs of mice, both femurs and tibias were removed. Both epiphyses were cut and bone marrow tissue was flushed out from the diaphysis until the bone became white/transparent. The tissue was suspended before separation of bone marrow cells from supernatant by centrifugation at 400 g, 4°C for 10 min. The supernatant was aspirated for BM-derived EV isolation and stored at 4°C until use (up to 2 hours). The pellet was suspended in 5 mL PBS and passed through a 40 µm nylon cell strainer to obtain single cell suspension.

Isolation of bone marrow-derived EVs

Bone marrow supernatant of 5-10 mice was pooled for having appropriate amount of EVs. Cell debris and apoptotic bodies were eliminated by centrifugation at 3000 g, 4°C for 15 min. Supernatant was aspirated and placed in a new clean centrifuge tube. EVs were isolated using ExoQuick-TC™ kit (System Biosciences) according to manufacturer's instruction. Briefly, 1 volume ExoQuick-TC™ solution was added to 5 volumes of supernatant and mixed well by rotating for 30 seconds. PBS control was prepared and treated similarly to the EVs. 5 volumes of 0.1 µm filtered PBS were mixed with 1 volume of ExoQuick-TC™ solution. The samples were incubated overnight at 4°C without percussion. Tubes with samples

were centrifuged at 1500 g, 4°C for 30 mins. The EV pellet was resuspended in 150-180 µL of 0.1 µm-filtered PBS. PD SpinTrap G-25 desalting columns (GE Healthcare, Life Science, WI, USA) were used to remove ExoQuick polymers (PEGs) from EV solution, based on manufacturer's protocol. Briefly, columns were pre-washed by centrifugation with 0.1 µm filtered PBS for 4 times then EV samples were places on the top of resin in the columns. EVs were eluted by centrifugation at 800 g, at room temperature (RT) for 2 min. To increase the amount of EVs the columns were washed once more with 150 µL 0.1 µm-filtered PBS by centrifugation at 800 g, RT for 2 min.

Bradford protein assay for measuring EV amount

To evaluate the overall broad quantity of EVs, Bradford protein assay was used which quantified the EVs based on the amount of proteins present on the surface of the vesicles. Absorbances were measured by a Synergy HT spectrofotometer (Biotek Instruments Inc. Winooski, VT, USA) at 595 nm. Protein concentrations were calculated based on available calibration curves.

Flow cytometry measurement

For BMCs and BM-derived EVs phenotyping the same antibody combinations were used. Half million BMCs and 40 µg of EV samples were used for one combination. BMCs, EV samples and PBS controls were labeled with appropriate antibodies for 30-60 mins at 4°C in the dark. The following directly labeled anti-mouse monoclonal antibodies were used for phenotypical analysis: CD90.2-APC and CD45-PE/Cy7 for lymphoid progenitors/-derived EVs, CD61-APC and CD41-FITC for megakaryocytic population/-derived EVs, Ter119-FITC for erythroid precursors/-derived EVs, CD11b-PE and Gr1-FITC for granulocytes/monocytes progenitors/-derived EVs, cKit (CD117)-APC for hematopoietic stem cells/-derived EVs, as well as CD29-PE and CD44-PE/Cy7 for mesenchymal progenitors/-derived EVs. All antibodies were purchased from BioLegend (San Diego, CA, USA) and Sony Biotechnology (San Jose, CA, USA). After incubation BMCs were washed in PBS and pelleted at 800 g, 4°C for 10 min, while EV samples and PBS controls were washed in 0.1 µm-filtered PBS and were pelleted by ultracentrifugation at 100,000 g, at 4°C for 70 min (Beckman Coulter, Brea, CA, USA) followed by immediate measurement and analysis of samples using a CytoFlex flow cytometer and CytExpert software (Beckman Coulter, Brea, CA, USA).

For size gating Megamix Plus-SSC, Megamix Plus-FSC (both purchased from BioCytex, Marseilles, France) commonly termed Gigamix beads and hollow organisilica beads (HOBs) (kind gift from Dr. Zoltán Varga, Research Center for Natural Sciences, Budapest, Hungary) were used.

Statistical Analysis

Data are presented as mean ± SD. Unpaired, one-sample Student's t-test and Mann-Whitney test were applied to determine statistical significance, using GraphPad Prism version 6.00 for Windows (GraphPad Software, La Jolla, CA, USA), if not stated otherwise. Data were considered statistically significant if p-value was lower than 0.05.

Results

a. Bone marrow cells decrease after irradiation

BM cells were isolated from BM of irradiated mice one day after radiation exposure. Cells were labelled with specific antibodies for BM subpopulations. Total cell numbers were determined and cell numbers of individual cell subpopulations were calculated using cytometry percentage data.

All of the measured cell populations decreased after 3 Gy irradiation at a great extent. The most drastic change was observed in the lymphoid (17-fold decrease compared to non-irradiated control mice), erythroid (9-fold decrease), monocyte-granulocyte (22.4-fold decrease) and megakariocyte (7.5-fold decrease) progenitor cells after 3 Gy exposure. The number of erythroid progenitors decreased significantly after 0.1 Gy, as well (Figure 16).

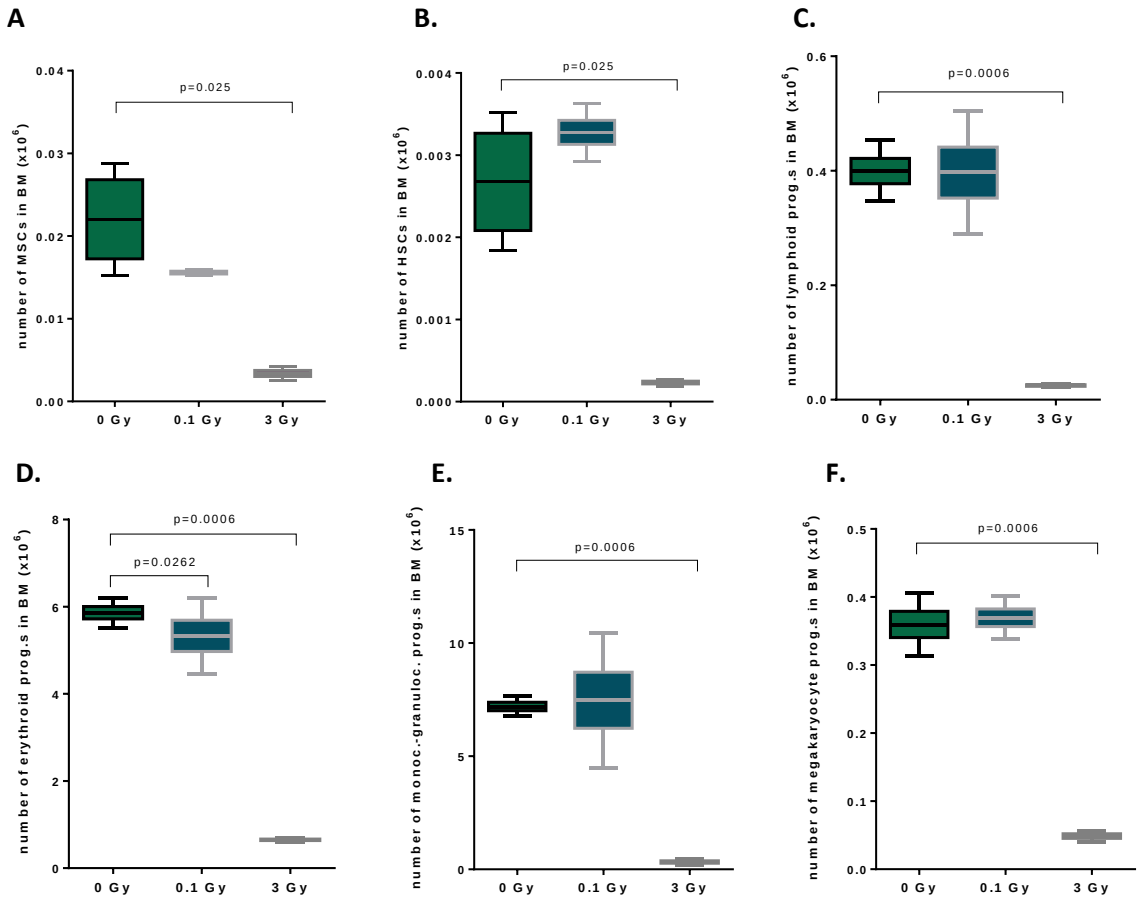

Figure 16. Changes in cell number of different bone marrow cell populations after irradiation. Bone marrow cells were isolated from non-irradiated and irradiated mice 24 h after exposure. Cells were labelled with antibodies against BM cell markers: CD29 and CD44 for Lin- MSCs (**A.**), cKit and SCA-1 for Lin- HSCs (**B.**), CD90.2 and CD45 for lymphoid progenitors (**C.**), Ter119 for erythroid progenitors (**D.**), CD11b and Gr1 for monocyte-granulocyte progenitors (**E.**), CD41 and CD61 for megakaryocyte progenitors (**F.**). Cell numbers were calculated using total BM cell numbers and percentage data of subpopulations. One column represents individual data of 6 mice. Mann-Whitney tests were performed using GraphPad software. Error bars mean SD, p values are shown above the graphs.

b. EV evaluation by flow cytometry

EVs were isolated from BM tissue in vivo using Exoquick-TC solution. For cytometry analysis the CytoFlex flow cytometer was used. With this cytometer we could visualise vesicles above 100 nm diameter directly using side scatter light from violet laser[20]. Next, we had to define a suitable size gate for the vesicles. Two different beads were used for validation: polystyrene beads (Gigamix) and hollow-organosilica beads (HOB). There was a notable difference between the location of the two gates (limited by the two type of beads) (Figure 17A).

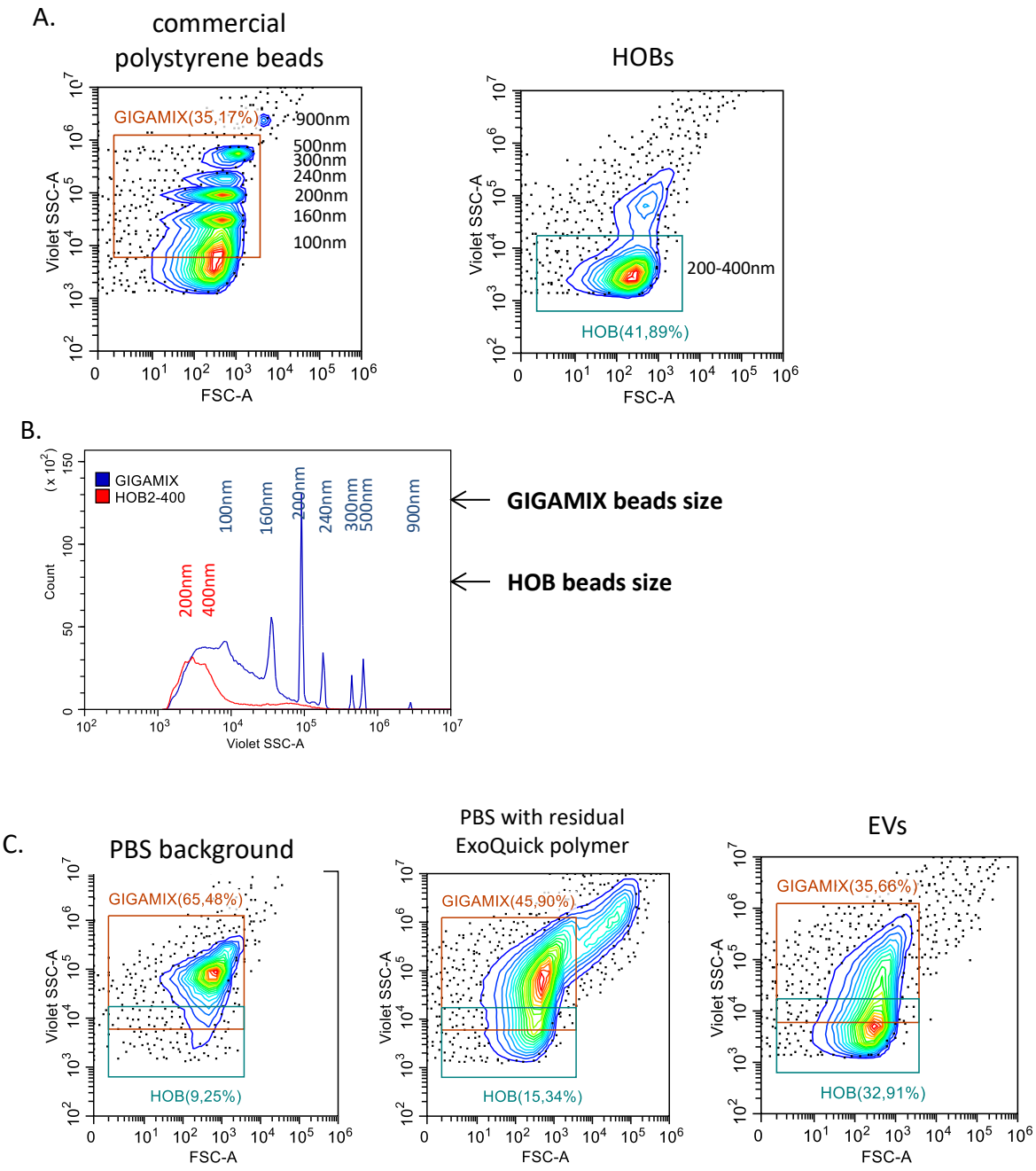

Figure 17. Gating strategy of extracellular vesicles (EVs). For determining size gate EVs were visualised via side scatter channel of violet laser. Two types of calibrating beads were used (**A.**): Megamix-SSC and Megamix-FSC (combined to Gigamix) and hollow-organosilica beads (HOBs). **B.** histogram overlay of the beads with the predicted vesicle sizes. **C.** buffers and biological samples with the 2 different size gates. Percentages show the gated fraction within all detected events.

Gigamix beads looked to locate in the area of bigger vesicles compared to HOB beads. Representing data on histogram plot showed that the size range of HOB beads (200-400 nm) was equivalent with the size below 100 nm of the Gigamix polystyrene beads (Figure 17B). Nevertheless, it was reported that the light scattering properties of the organosilica beads are closer to the light scattering of EVs than that of polystyrene beads [21]. Therefore we used both gates to indentify particular 'smaller' and 'bigger' vesicles, although these two gates had overlapping regions. According to our results, EV samples were distinguishable from the buffer controls (backgrounds) based on the ratio of the events within the Gigamix and the HOB gates (Figure 17C).

c. Changes in ratio of EVs released by BM cells after irradiation

First, isolated EVs were labeled with EV-specific antibodies (CD9, CD63 and CD81). Within Gigamix or HOB events EV-marker positivity was specified and we analysed further those events that were gated in this regard. EV-marker positivity was marked according to the 'PBS with residual polymer' control (Figure 18).

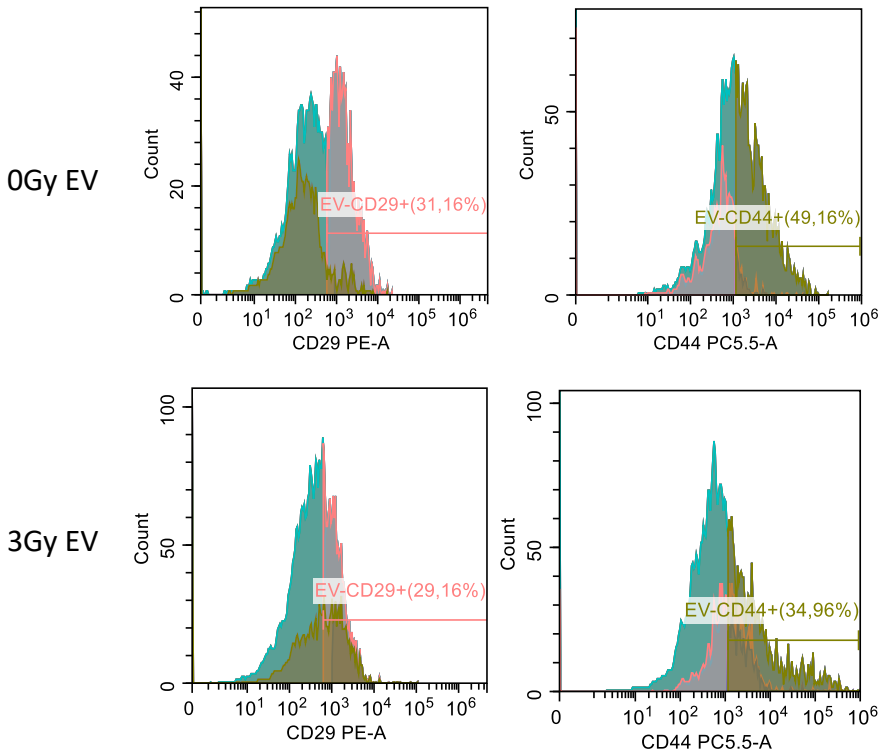

Figure 18. Representative figure of CD29 and CD44 histograms. EVs were isolated from bone marrow tissue of un-irradiated and irradiated mice and were labelled with antibodies against EV-specific proteins (CD9, CD63 and CD81) and typical proteins of bone marrow cell populations (here: CD29 and CD44 for mesenchymal stem cells (MSCs)).

Most EVs expressed the integrins typical for MSCs (CD29 and CD44) (CD29 positivity 30.5%, 34.46% and 13.86% within 'smaller' vesicles in 0 Gy, 0.1 Gy and 3 Gy samples, respectively and CD44 positivity 42.07%, 47.06% and 24.71% within 'smaller' vesicles in 0 Gy, 0.1 Gy and 3 Gy samples, respectively), thus MSCs supposed to be a subpopulation releasing the most EVs into the BM microenvironment (Table 13).

A	smaller vesicles'								
	CD29	CD44	cKit	CD90.2	Ter119	CD11b	Gr-1	CD41	CD61
0 Gy	30.5 (±5.64)	42.07 (±18.2)	0.832 (±0.41)	4.294 (±2.71)	0.227 (±0.17)	3.157 (±1.05)	4.057 (±1.262)	5.537 (±2.74)	0.087 (±0.036)
0.1 Gy	34.46 (±9.4)	47.06 (±14.2)	0.653 (±0.34)	11.25 (±1.14)*	0.328 (±0.17)	3.19 (±1.39)	6.347 (±1.36)	11.44 (±5.25)	0.103 (±0.012)
3 Gy	13.86 (±4.05)***	24.71 (±9.75)*	3.478 (±1.52)	9.146 (±4.44)	1.345 (±0.44)*	3.748 (±0.49)	8.18 (±4.31)	9 (±3.89)	0.365 (±0.11)

B	larger vesicles'								
	CD29	CD44	cKit	CD90.2	Ter119	CD11b	Gr-1	CD41	CD61
0 Gy	30.41 (±16.33)	47.22 (±21.14)	2.125 (±1.5)	7.33 (±2.11)	1.723 (±0.71)	9.353 (±2.52)	6.8 (±0.88)	8.89 (±6.26)	0.64 (±0.37)
0.1 Gy	23.02 (±7.43)	23.93 (±9.98)*	2.373 (±1.05)	7.44 (±3.65)	1.247 (±0.41)	11.12 (±3.7)	11.3 (±6.65)	12.75 (±8.1)	0.61 (±0.39)
3 Gy	12.97 (±8.84)*	9.24 (±5.02)***	4.36 (±2.3)	6.19 (±3.24)	2.22 (±1.58)	15.62 (±4.96)	15.64 (±5.4)*	21 (±5.21)	2,46 (±1.7)

Table 13. Percentage of EVs expressing typical bone marrow cell markers. EVs were isolated from bone marrow tissue and labelled with EV-specific markers followed by antibodies against typical bone marrow cell proteins. Data represent percentages within EV-marker positive events of 'smaller vesicles' (**A**) and 'larger vesicles' (**B**). Four mice were pooled for one sample and min. 4 paralells were used for statistical analysis. ± mean SD, changes are significant if *p<0.05, **p<0.01, ***p<0.005 compared to 0 Gy.

Decreasing of MSC-derived EVs after irradiation was in consistency with the reduction of living MSC pool in the BM (Figure 4). Nevertheless, despite of shrinking subpopulations, several progenitor cells seemed to release more EVs after irradiation than in control (0 Gy) mice. Ratio of eythroid progenitors-derived EVs (with Ter119 positivity) increased almost 8-times after 3 Gy irradiation compared to the 0 Gy samples. Gr-1 positive EVs (released by granulocyte progenitors) showed 4.55-fold increase in 3 Gy samples than the control ones (Figure 19). Moreover, these changes were present for the release of both 'smaller' and 'larger' vesicles.

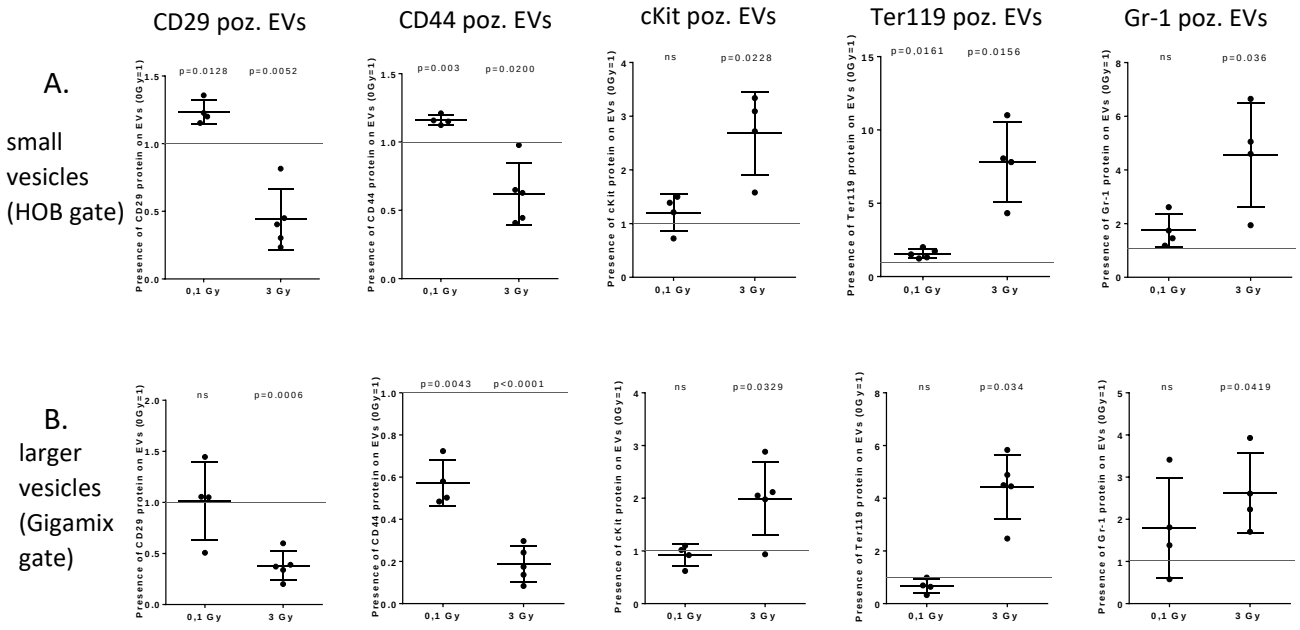

Figure 19. Changes in ratio of EVs released by different bone marrow cell populations. EVs were isolated from bone marrow tissue and labelled with EV-specific antibodies followed by labeling with typical proteins against bone marrow subpopulations. EVs were measured in 2 size gates: one for smaller vesicles (HOB gate) (**A.**), one for larger vesicles (Gigamix gate) (**B.**). CD29 and CD44 positive EVs were released by MSCs, cKit positive EVs by hematopoietic stem cells (HCSs), Ter119 positive EVs by erythropoietic progenitors and Gr-1 by granulocyte progenitors. One dot represents one individual sample of BM from 4 mice pooled. One-sample t-tests were performed using GraphPad software. Error bars mean SD, p values are shown above the graphs. Only significant changes are represented.

Discussion and conclusion

Flow cytometry is a forceful method for identifying and characterizing cells and smaller particles, including EVs. However, for single-vesicle evaluation flow cytometers should have higher detection sensitivity with perception threshold reaching 500 nm size. The next step in the way of particle flow detection, the standardization of vesicle size within detected events became possible by introduction of calibrating beads[22]. In our study, determining the size gate of EVs was performed by two types of calibrations beads. First, Megamix Plus-SSC and Megamix Plus-FSC beads were mixed together (formed Gigamix) and size gate of vesicles was determined from size 100 nm beads to size 500 nm beads. This method is generally accepted by several groups [23 24], however, recently its accuracy became questionable [9 25]. The basic of these theories is the fact that artificial beads and biological vesicles have quite different refractive features e.g. EVs scatter light approximately 10-fold less efficiently than polystyrene beads [26 9]. Chandler et al.'s study demonstrated that 400 nm polystyrene beads likely correlate to 1,000 nm microparticles[26]. Erdbrugger et al. have confirmed this using 200 nm liposomes and 200 nm polystyrene beads[27]. These findings are in agreement with our results, as we demonstrated that the gate/position on dot plot of polysyrene beads with size 100 nm could mean the position of hollow-organosilica bead population with 200-400 nm size. Therefore, beside Gigamix beads, we used HOB beads for gating EVs. HOBs were a kind gift of Dr. Zoltán Varga from Research Center for Natural Sciences (Budapest, Hungary). These beads proved to have very similar light scattering properties to biological vesicles[21], therefore they are superior to polystyrene beads in size determining of EVs by flow cytometry. As we could see during measurements, our vesicle samples had more events in gate marked by HOBs, which could justify the usage of HOBs and evalute isolated vesicles also.

Bone marrow cells are extremely radiosensitive, thus high dose irradiation leads to massive cell death within BM stem and progenitor cells, as it was shown in our previous study in C57Bl6 mice[19]. Here, we demonstrated the same cell loss after 3 Gy irradiation in CBA male mice. Moreover, we found that number of erythroid progenitors in BM decreased significantly after 0.1 Gy irradiation, as well.

Identifying EVs released by BM cell populations was based on the presence of typical BM cell proteins on the membrane surface of EVs. However, several of these proteins are primarily involved in cell-cell and cell-matrix communication within the BM niche and are not exclusively related to one cell type. These integrins maintain adhesion, migration and survival of HSCs and hematopoietic progenitor cells. In this regard, CD29 (β1 integrin), was found to promote the initial contact of HSCs to MSCs[28] as a cytoadhesive molecule, and CD61 (β3 integrin) expression was shown to be a marker for long-term repopulation of HSCs *in vivo*[29 30]. Furthermore, Liu et al. reviewed integrins on osteoblast-EVs [31] also. We used one marker positivity as well to identify the cell of origin of EVs, not only double positivity as in case of BM cells. This approach was used by others as well for example EVs expressing either CD61 or CD41 or CD235 and not necessarily all three markers were considered to be of platelet origin [9 32-34].

In conclusion, we found different patterns in changing EV secretion of bone marrow cells after irradiation. First, as seen in the case of MSCs, the amount of released EVs decreased with the decline of cell number after 3 Gy irradiation. The less surviving cells, the less EVs secreted, thus we can assume that there was no change in EV release per cell after irradiation. On the other hand, in case of HSCs, erythroid and granulocyte progenitors, despite of decreasing cell number after 3 Gy exposure, the ratio and percentage of EVs released by these cells increased significantly compared to those in the control mice. From these results we can conclude that HSCs, erythroid and granulocyte progenitors released more EVs after irradiation per cell. In addition, according to our data, MSCs released significantly more EVs after 0.1 Gy irradiation compared to control. This finding could be explained by the role of MSCs in promoting bone regeneration and radiation damage repair after irradiation. MSC-secrotome, including EVs proved to foster osteogenic differentiation of recipient MSCs [35].

References

1. Richard S, Amy L, Ming-Chung L, et al. Analysis of Gene Expression Data Using BRB-Array Tools. *Cancer Informatics* 2007;3:117693510700300022. doi: 10.1177/117693510700300022
2. Vlachos IS, Zagganas K, Paraskevopoulou MD, et al. DIANA-miRPath v3.0: deciphering microRNA function with experimental support. *Nucleic Acids Research* 2015;43(Web Server issue):W460-W66. doi: 10.1093/nar/gkv403
3. Krist B, Florczyk U, Pietraszek-Gremplewicz K, et al. The Role of miR-378a in Metabolism, Angiogenesis, and Muscle Biology. *Int J Endocrinol* 2015;2015:281756-56. doi: 10.1155/2015/281756 [published Online First: 2015/12/29]
4. Zhou H, Suzuki M, Randers-Pehrson G, et al. Radiation risk to low fluences of alpha particles may be greater than we thought. *Proc Natl Acad Sci U S A* 2001;98(25):14410-5. doi: 10.1073/pnas.251524798 [published Online First: 2001/12/06]
5. Shao C, Stewart V, Folkard M, et al. Nitric oxide-mediated signaling in the bystander response of individually targeted glioma cells. *Cancer Res* 2003;63(23):8437-42. [published Online First: 2003/12/18]
6. Philipp J, Azimzadeh O, Subramanian V, et al. Radiation-Induced Endothelial Inflammation Is Transferred via the Secretome to Recipient Cells in a STAT-Mediated Process. *J Proteome Res* 2017;16(10):3903-16. doi: 10.1021/acs.jproteome.7b00536 [published Online First: 2017/08/30]
7. Szatmari T, Hargitai R, Safrany G, et al. Extracellular Vesicles in Modifying the Effects of Ionizing Radiation. *Int J Mol Sci* 2019;20(22) doi: 10.3390/ijms20225527 [published Online First: 2019/11/09]
8. Szatmari T, Persa E, Kis E, et al. Extracellular vesicles mediate low dose ionizing radiation-induced immune and inflammatory responses in the blood. *Int J Radiat Biol* 2019;95(1):12-22. doi: 10.1080/09553002.2018.1450533 [published Online First: 2018/03/14]
9. van der Pol E, de Rond L, Coumans FAW, et al. Absolute sizing and label-free identification of extracellular vesicles by flow cytometry. *Nanomedicine* 2018;14(3):801-10. doi: 10.1016/j.nano.2017.12.012 [published Online First: 2018/01/09]
10. 1Aatonen MT, Ohman T, Nyman TA, et al. Isolation and characterization of platelet-derived extracellular vesicles. *J Extracell Vesicles* 2014;3 doi: 10.3402/jev.v3.24692 [published Online First: 2014/08/26]
11. Lasser C, Eldh M, Lotvall J. Isolation and characterization of RNA-containing exosomes. *J Vis Exp* 2012(59):e3037. doi: 10.3791/3037 [published Online First: 2012/01/20]
12. Hoshino A, Costa-Silva B, Shen TL, et al. Tumour exosome integrins determine organotropic metastasis. *Nature* 2015;527(7578):329-35. doi: 10.1038/nature15756 [published Online First: 2015/11/03]
13. Tian T, Zhu YL, Hu FH, et al. Dynamics of exosome internalization and trafficking. *J Cell Physiol* 2013;228(7):1487-95. doi: 10.1002/jcp.24304 [published Online First: 2012/12/21]
14. Ratajczak J, Wysoczynski M, Hayek F, et al. Membrane-derived microvesicles: important and underappreciated mediators of cell-to-cell communication. *Leukemia* 2006;20(9):1487-95. doi: 10.1038/sj.leu.2404296 [published Online First: 2006/06/23]
15. Gyorgy B, Szabo TG, Pasztoi M, et al. Membrane vesicles, current state-of-the-art: emerging role of extracellular vesicles. *Cell Mol Life Sci* 2011;68(16):2667-88. doi: 10.1007/s00018-011-0689-3 [published Online First: 2011/05/12]
16. Hazawa M, Tomiyama K, Saotome-Nakamura A, et al. Radiation increases the cellular uptake of exosomes through CD29/CD81 complex formation. *Biochem Biophys Res Commun* 2014;446(4):1165-71. doi: 10.1016/j.bbrc.2014.03.067 [published Online First: 2014/03/29]
17. Beer L, Seemann R, Ristl R, et al. High dose ionizing radiation regulates micro RNA and gene expression changes in human peripheral blood mononuclear cells. *BMC Genomics* 2014;15:814. doi: 10.1186/1471-2164-15-814 [published Online First: 2014/09/27]
18. Yentrapalli R, Merl-Pham J, Azimzadeh O, et al. Quantitative changes in the protein and miRNA cargo of plasma exosome-like vesicles after exposure to ionizing radiation. *International Journal of Radiation Biology* 2017;93(6):569-80. doi: 10.1080/09553002.2017.1294772

19. Szatmári T, Kis D, Bogdándi EN, et al. Extracellular Vesicles Mediate Radiation-Induced Systemic Bystander Signals in the Bone Marrow and Spleen. *Frontiers in Immunology* 2017;8:347. doi: 10.3389/fimmu.2017.00347
20. Brittain GCt, Chen YQ, Martinez E, et al. A Novel Semiconductor-Based Flow Cytometer with Enhanced Light-Scatter Sensitivity for the Analysis of Biological Nanoparticles. *Sci Rep* 2019;9(1):16039. doi: 10.1038/s41598-019-52366-4 [published Online First: 2019/11/07]
21. Varga Z, van der Pol E, Palmai M, et al. Hollow organosilica beads as reference particles for optical detection of extracellular vesicles. *J Thromb Haemost* 2018 doi: 10.1111/jth.14193 [published Online First: 2018/06/08]
22. Lacroix R, Robert S, Poncelet P, et al. Overcoming limitations of microparticle measurement by flow cytometry. *Semin Thromb Hemost* 2010;36(8):807-18. doi: 10.1055/s-0030-1267034 [published Online First: 2010/11/05]
23. Poncelet P, Robert S, Bailly N, et al. Tips and tricks for flow cytometry-based analysis and counting of microparticles. *Transfus Apher Sci* 2015;53(2):110-26. doi: 10.1016/j.transci.2015.10.008 [published Online First: 2015/11/26]
24. Al-Mayah AHJ, Irons SL, Pink RC, et al. Possible role of exosomes containing RNA in mediating nontargeted effect of ionizing radiation. *Radiation Research* 2012;177(5):539-45.
25. Simonsen JB, Larsen JB, Hempel C, et al. Unique Calibrators Derived from Fluorescence-Activated Nanoparticle Sorting for Flow Cytometric Size Estimation of Artificial Vesicles: Possibilities and Limitations. *Cytometry A* 2019;95(8):917-24. doi: 10.1002/cyto.a.23797 [published Online First: 2019/05/24]
26. Chandler WL, Yeung W, Tait JF. A new microparticle size calibration standard for use in measuring smaller microparticles using a new flow cytometer. *J Thromb Haemost* 2011;9(6):1216-24. doi: 10.1111/j.1538-7836.2011.04283.x [published Online First: 2011/04/13]
27. Erdbrugger U, Rudy CK, Etter ME, et al. Imaging flow cytometry elucidates limitations of microparticle analysis by conventional flow cytometry. *Cytometry A* 2014;85(9):756-70. doi: 10.1002/cyto.a.22494 [published Online First: 2014/06/07]
28. Teixido J, Hemler ME, Greenberger JS, et al. Role of beta 1 and beta 2 integrins in the adhesion of human CD34hi stem cells to bone marrow stroma. *J Clin Invest* 1992;90(2):358-67. doi: 10.1172/JCI115870 [published Online First: 1992/08/01]
29. Umemoto T, Yamato M, Shiratsuchi Y, et al. CD61 enriches long-term repopulating hematopoietic stem cells. *Biochem Biophys Res Commun* 2008;365(1):176-82. doi: 10.1016/j.bbrc.2007.10.168 [published Online First: 2007/11/07]
30. Umemoto T, Yamato M, Shiratsuchi Y, et al. Expression of Integrin beta3 is correlated to the properties of quiescent hemopoietic stem cells possessing the side population phenotype. *J Immunol* 2006;177(11):7733-9. doi: 10.4049/jimmunol.177.11.7733 [published Online First: 2006/11/23]
31. Liu M, Sun Y, Zhang Q. Emerging Role of Extracellular Vesicles in Bone Remodeling. *J Dent Res* 2018;97(8):859-68. doi: 10.1177/0022034518764411 [published Online First: 2018/03/23]
32. de Rond L, van der Pol E, Hau CM, et al. Comparison of Generic Fluorescent Markers for Detection of Extracellular Vesicles by Flow Cytometry. *Clin Chem* 2018;64(4):680-89. doi: 10.1373/clinchem.2017.278978 [published Online First: 2018/02/18]
33. Arraud N, Linares R, Tan S, et al. Extracellular vesicles from blood plasma: determination of their morphology, size, phenotype and concentration. *J Thromb Haemost* 2014;12(5):614-27. doi: 10.1111/jth.12554 [published Online First: 2014/03/13]
34. Ponomareva AA, Nevzorova TA, Mordakhanova ER, et al. Intracellular origin and ultrastructure of platelet-derived microparticles. *J Thromb Haemost* 2017;15(8):1655-67. doi: 10.1111/jth.13745 [published Online First: 2017/06/01]
35. Liu S, Liu D, Chen C, et al. MSC Transplantation Improves Osteopenia via Epigenetic Regulation of Notch Signaling in Lupus. *Cell Metab* 2015;22(4):606-18. doi: 10.1016/j.cmet.2015.08.018 [published Online First: 2015/09/15]